Structural insights into the recruitment of viral Type 2 IRES to ribosomal preinitiation complex for protein synthesis

Deepakash Das and Tanweer Hussain

Department of Developmental Biology and Genetics, Indian Institute of Science, Bengaluru, INDIA. PIN-560012

*Correspondence: hussain@iisc.ac.in

Abstract

Picornaviruses employ internal ribosome entry sites (IRESs) in their genomic RNA to hijack the host's translational machinery. The picornavirus, Encephalomyocarditis virus, employs a type 2 IRES present in its 5'UTR and requires 43S ribosomal preinitiation complex (PIC), the central domain of eukaryotic initiation factor (eIF) 4G, eIF4A, and an essential ITAF (IRES trans-acting factor)-polypyrimidine tract binding protein 1 (PTB1) to form 48S PIC. In this study, we have used cryo-electron microscopy (cryo-EM) to determine the structure of EMCV IRES-bound mammalian 48S PIC in a scanning-arrested closed state at the start codon. The EMCV IRES domains contacts initiator tRNA ($tRNA_i$) and 40S head at the inter-subunit interface, which reveals an altogether unique mechanism used by viruses to capture host translational machinery for its protein synthesis. The $tRNA_i$ is held away from the 40S body in contrast to canonical cap-dependent translation while the domain I apical region of EMCV IRES mimics 28S rRNA of 60S to interact with 40S ribosomal head proteins- uS13 and uS19. The structural analysis account for numerous biochemical studies on Type 2 IRES and shows how Type 2 IRES interacts with 43S PIC to form 48S PIC. This study provides mechanistic insights for understanding EMCV IRES-mediated translation initiation, which could be extrapolated to other IRESs sharing similar motifs and factor requirements including type 1 viral IRESs.

Introduction:

Eukaryotic translation initiation occurs in two different modes- Cap-dependent and Cap-independent. Cap-dependent translation initiation in eukaryotes can be divided into four major steps- (i) formation of 43S ribosomal PIC [40S subunit in complex with eIF1, eIF1A, eIF3, eIF5 and ternary complex (eIF2-GTP-tRNA$_i$)]; (ii) recruitment of 43S PIC to 5'end of capped mRNA, mediated by eIF4F complex (formed by eIF4E,eIF4G and eIF4A) yielding 48S complex (48S PIC); (iii) scanning of 5' untranslated region (UTR) of mRNA and start codon recognition; and (iv) joining of large 60S ribosomal subunit to form elongation-competent 80S ribosomal complex. Among these, major rate-limiting steps include- the regulation of available tRNA$_i$ as the ternary complex (eIF2.GTP.Met-tRNA$_i$) and recruitment of mRNA on 43S PIC (*Jackson et al 2010; Brito Querido et al 2024*). Cryo-EM studies on eukaryotic canonical 48S PICs from yeast (*Hussain et al 2014; Llacer et al 2015*) to humans (*Eliseev et al 2018; Simonetti et al 2020; Brito Querido et al 2020; Yi et al 2022; Brito Querido et al 2024; Petrychenko et al 2024*) have revealed various interactions among the initiation factors, mRNA, and ribosome in scanning (P_{OUT} or open) state and scanning-arrested (P_{IN} or closed) states. In mammals, 48S PIC formation is mediated by the interaction of eIF3 and eIF4G (*Villa et al 2013*) and recent attempts to understand the mammalian canonical 48S PIC could capture interactions of eIF4 proteins (eIF4G and eIF4A) with eIF3 (*Brito Querido et al 2020; Brito Querido et al 2024*).

Alternatively, several positive strand RNA viruses use Internal Ribosome Entry Sites (IRESs), which are internal cis-acting sequences present in 5' UTR of mRNA that drive the assembly of translation initiation complex without the requirement of 7-methylguanosine cap (*Martínez-Salas et al 2018*), initially reported in picornaviruses such as poliovirus (PV) and encephalomyocarditis virus (EMCV) RNA genome (*Jang et al 1988; Pelletier and Sonenberg, 1988; Trono et al 1988*). As of 2020, the IRESbase database reported 1328 IRESs, out of which 554 were viral IRESs from 198 viruses (*Zhao et al 2020*). These RNA elements have unique secondary and tertiary structures, which allows them to hijack the host translational machinery and promote translation initiation internally by recruitment of host ribosome, canonical eIFs, and IRES trans acting factors (ITAFs) via multiple RNA–RNA and RNA–protein interactions (*Lee et al 2017; Martinez-Salas et al 2018*). The IRESs lack sequence homology and enfolds different structural organization, thus requiring different eIFs for the assembly of

48S PICs (*Jackson et al 2010*). The type 1 IRES (represented by PV) and type 2 IRES (EMCV) requires almost all eIFs, except eIF4E or N terminal of eIF4G for the formation of 48S PIC (*Lozano and Martinez-Salas, 2015)*. However, initiation on the latter does not require scanning for start codon recognition (*Kaminski et al 1994; Sweeney et al 2014)*. The type 3 IRES (Hepatitis C virus- HCV) does not require eIF4 factors or scanning for 48S PIC formation (*Niepmann and Gerresheim 2020*). The type 4 IRES (Cricket paralysis virus- CrPV intergenic IRES) initiates without the requirement of any eIFs and $tRNA_i$ (*Johnson et al 2017*). The HCV IRES and CrPV intergenic IRES directly interacts with host 40S ribosome, however they differ in their mechanism of attachment. Where, the CrPV IRES (type 4) mimics anticodon-codon interaction via pseudoknot 1 to bind with ribosome in an elongation-competent state (*Petrov et al 2016; Fernandez et al 2014*) the HCV IRES (type 3) binds to the solvent side of 40S subunit by replacing eIF3 and directly interacts with expansion segment (ES7) of 18S rRNA and ribosomal proteins near mRNA exit channel, thus placing the initiation codon at the P-site (*Hashem et al 2013; Niepmann and Gerresheim 2020; Brown et al 2022*). While the structures of ribosome-bound type 4 (*Spahn et al 2004; Fernandez et al 2014; Muhs et al 2015; Murray et al 2016; Pisareva et al 2018; Acosta-Reyes et al 2019; Abaena et al 2020*) and type 3 IRES (*Spahn et al 2004; Boehringer et al 2005; Hashem et al 2013; Yamamoto et al 2014; Quade et al 2015; Yamamoto et al 2015; Yokoyama et al 2019; Brown et al 2022*) have been determined, there is no structural information about Type 2 and Type 1 IRES and their mode of recruitment to 48S PIC.

The 5'UTR of EMCV, genera Cardiovirus and Picornaviridae family (*International Committee on Taxonomy of Viruses Executive Committee, 2020*) folds into various stem-loops numbered D-L and, domains H-L, followed by initiation codon at the 834th residue (~450 nucleotides in length) makes a functional IRES moiety (*Carocci et al 2012*). It requires the core of 43S PIC, the central domain of eIF4G, eIF4A, and an essential ITAF-polypyrimidine tract binding protein 1 (PTB1) and the presence of eIF4B enhances 48S formation (*Hellen and Wimmer 1995; Martinez-Salaz et al 2018; Sweeney et al 2014*). Functional characterization of these domains showed H, and I interact with 40S ribosomal subunit (*Chamond et al 2014*), and J-K domain recruits eIF4G, enhanced by eIF4A (*Pestova et al 1996; Lomakin et al 2000*). The structure of J-K domain-eIF4G1(HEAT1)-eIF4A revealed that positively charged patches on the eIF4G1-HEAT1 domain interact with two separated negatively charged clefts (in J and St domain)

without perturbing its innate function of recruiting eIF4A (*Imai et al 2016; Imai et al 2023*). The binding sites for PTB1 were revealed to be dispersed, encompassing H to L domains (*Kafasla et al 2009*). These domains function as a single entity to form 48S PIC and any mutation in conserved IRES motifs can drastically affect the translation rates (*Fernández-Miragall et al 2009; Fernández et al 2011*). For example, the RAAA and GNRA loop in the I domain of type 2 IRES are crucial for IRES activity (*Robertson et al 1999*), and the GNRA loop is also found in other IRES families such as type 1 (poliovirus) and type 5 (Aichi virus A) picornaviruses (*Abdullah et al 2023*). The inherent flexibility within the IRES domains provide a challenge for structural studies of full length IRES and to capture IRES in the context of 48S PIC. EMCV IRES can independently interact with 40S subunit without any eIFs (*Chamond et al 2014*) and does not require scanning to recognize the start codon (*Pestova et al 1996*), unlike type 1 IRESs which scans for the start codon (*Sweeney et al 2014*). Besides, EMCV IRES can form 48S PIC with HEAT1-eIF4G without the requirement of eIF4G residues 1015-1104 that are known to interact with eIF3 (*Lomakin et al 2000*). These residues are indispensable in case of canonical initiation on capped mRNAs and for type 1 IRESs (*Villa et al 2013; Sweeney et al 2014*). However, how EMCV IRES interacts with 40S subunit or what are the molecular interactions essential to form the EMCV IRES-48S PIC remains a question.

In this study we have used pull down assay to isolate EMCV IRES-bound 48S PIC from Rabbit Reticulocyte Lysate (RRL) and subjected the complex to cryo-electron microscopy (Cryo-EM) analysis. The cryo-EM map of EMCV IRES-bound 48S PIC, henceforth mentioned as EMCV IRES-48S PIC, shows densities corresponding to EMCV IRES domains that reveals how EMCV IRES contacts the ternary complex and 40S head at the inter-subunit interface. The structural details presented here accounts for numerous biochemicals studies that have been reported earlier on Type 2 IRES. Furthermore, the structural analysis suggests how Type 2 IRES would interact with 43S PIC to form 48S PIC. Importantly, the study reveals a unique strategy used by viral IRES to capture host translational apparatus for making viral polypeptide.

Results:

1. Overview and features of EMCV IRES-48S PIC

To isolate 48S PIC on EMCV IRES, we used a Talon affinity based pull down from nuclease-treated RRL. EMCV IRES RNA used harboured residues from 280 to 905 with AUG (start codon) at 834th position. PTB1 was recombinantly overexpressed with a N-terminal 6X His tag, followed by a 3C protease cleavage site. PTB1 was incubated with the IRES, followed by RRL addition and 48S PIC was stalled using GMP-PnP. The complex was eluted from Talon matrix employing 3C protease cleavage and pelleted (Sup. Fig. 1.1 A). The EMCV IRES-48S PIC was subsequently analysed by Cryo-EM. The processed data yielded 3 major classes- (i) 40S without any factors- Map A, (ii) 40S-IRES-tRNA$_i$- Map B, and (iii) 40S-IRES-ternary complex-Map B1, namely, EMCV IRES-48S PIC (Sup. Fig. 1.1 B). Map B and Map B1 has an overall resolution of 4.6Å and 5.0Å, respectively (Sup. Fig. 1.1 B). The core of 40S is at around 4.0Å and the local resolution across the maps were largely in the range of 4.0-8Å (Sup. Figs. 1.2 A and B). Only the extreme tip of beak of 40S in Map B1 (Sup. Fig. 1.2 A) and ends of IRES and eIF2γ is around 12Å in Map B2 (Sup. Figs 1.2 B).

The cryo-EM densities in EMCV IRES-48S PIC corresponds to 40S, tRNA$_i$, eIF2α, eIF2γ and RNA in the mRNA channel along with an extra density connecting 40S ribosomal head to tRNA$_i$ (Fig. 1A-B). However, it lacks distinct density for PTB1, eIF4G, eIF4A, and eIF3 and hence these factors are not modelled. Since nuclease-treated RRL lacked endogenous RNA, the presence of density for mRNA in the channel indicates trapping of EMCV IRES in 48S PIC. Also, the density connecting 40S head to tRNA$_i$ in Map B and B1 could be assigned to a double stranded RNA structure found in EMCV IRES (Fig. 1A-B).

Besides, an extra density is evident at the mRNA entry site, contacting 40S ribosomal proteins-uS3, eS10, and uS5 and h16 (Helix 16) of 18S rRNA (Sup. Fig. 1.2 C). In the human 48S PIC, this region positions eIF3g-RRM (RNA recognition motif) and downstream ORF (Sup. Fig.1.2 D) (*Brito Querido et al 2020; Brito Querido et al 2024)*. We anticipate this extra density in EMCV IRES-48S PIC could be contributed by downstream ORF, however, it's difficult to assign it to eIF3g-RRM due to lack of eIF3 (core/peripheral) density. Furthermore, our recent study on

interaction of yeast eIF4B with 40S ribosome suggested occupancy of eIF4B (N terminal-RRM) in the same region (*Datey et al 2025*), which opens up the possibility of mammalian eIF4B-NT-RRM to bind to this region in the absence of eIF3, although in the human 48S PIC eIF4B was tentatively positioned slightly away from this location (*Brito Querido et al 2024)*. An interesting possibility could be positioning one of the RRM domains of PTB1 bound to UCUUU sequence of 18S rRNA (PTB1 can bind to UCUUU sequence- *Maris et al 2020*) present at the tip of h16 (528-532 nucleotides) of 18S rRNA. An extra density in the same position is also present in Map A (40S without EMCV IRES or factors- Sup. Fig. 1.2 E) as well, and PTB1 was used as a bait for the pull-down, therefore, this density may be contributed by PTB1-RRM interacting with h16 of 18S rRNA.

Figure 1

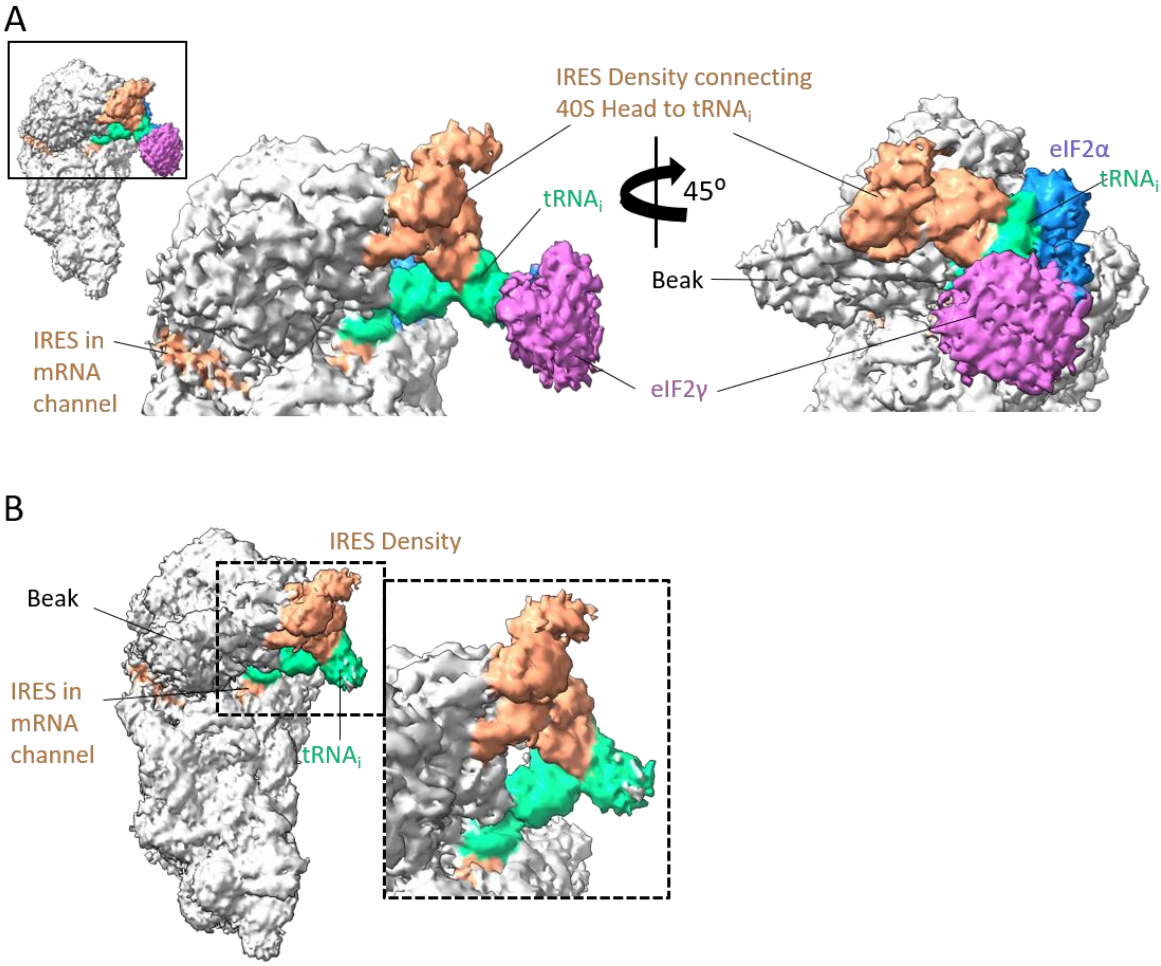

Figure 1 (A) Different views of EMCV IRES-48S PIC (Map B1) by 45° rotation along one axis. The map shows densities assigned to 40S ribosome, RNA (in channel), ternary complex and IRES density at the inter-subunit region of head. **(B)** View of Map B and zoomed view of densities corresponding to IRES and $tRNA_i$.

Table 1: Cryo-EM data and model statistics

Data collection	**Map A- 40S without factors**	**Map B- 40S-tRNA$_i$-EMCV IRES**	**Map B1- 40S-tRNA$_i$-EMCV IRES-eIF2α-eIF2γ**
Microscope	Talos Arctica		
Camera	Gatan K2 Summit Direct Detector		
Magnification	36000X		
Voltage (kV)	200		
Electron dose (e^-/Å$^{2)}$	50-55		
Defocus range	-2 to -0.5		
Pixel size (Å)	1.17		
Number of micrographs	22549		
Cryo-EM reconstruction			
Final number of particles	125503	55231	28439
Point group symmetry	C1	C1	C1
Fsc threshold	0.143	0.143	0.143
Map overall resolution(Å)	4.51	4.55	5.01
Resolution metric	Gold-Standard FSC	Gold-Standard FSC	Gold-Standard FSC
Sharpening B factor(Å^2)	-153.5	-117.9	-122.3
Atomic model refinement			
Resolution (0.5) (Å)	5.0	5.4	6.0
D FSC model (0/0.143/0.5)	4.4/4.5/5.0	4.4/4.5/5.4	4.9/4.9/6.0
Initial models used	6YAN	6YAN; 8OZ0	6YAN; 8OZ0
CC overall			
CC(mask)/(box)/(peaks)/(volume)	0.73/0.83/0.72/0.66	0.77/0.84/0.71/0.77	0.76/0.84/0.70/0.75
Molprobity score	2.3	2.28	2.31
Clash score	19.08	19.09	21.24
No. of atoms/ No. of residues			
Chains	39	41	43
Total atoms (Hydrogens:0)	76455	80057	85830
No. of residues-Proteins/Nucleotides	4916/1744	4918/1912	5660/1912
Bond (RMSD) Lengths (Å)	0.002	0.003	0.003
Bond (RMSD) Angles (°)	0.658	0.650	0.665
Ramachandran plot (%)			
Outliers	0.21	0.27	0.21
Allowed	8.94	8.21	7.90
Favored	90.86	91.52	91.89
Rotamer outliers (%)	0.02	0.02	0.00
Cβ outliers (%)	0.00	0.00	0.00
CaBLAM outliers (%)	6.09	5.82	5.46

2. The EMCV IRES-48S PIC is trapped in a closed conformation

In EMCV IRES, A-834-G-836 forms the start codon *(Kaminski et al 1994; Hellen and Wimmer 1995; Pestova et al 1996)* and it is present in a Kozak context (CRCCaugG; R is a purine) *(Kozak 1989)*, where the -3 position is A-831 and +4 is G-837 (Sup. Fig. 2D). Based on these, we anticipate the 834th AUG base-paired to the anticodon (Fig. 2A) and the flanking residues were added as per the sequence (Sup. Fig. 2D). The recognition of the start codon at the P-site by $tRNA_i$ leads to accommodation of ternary complex and 48S PIC adopts a P_{IN} state in contrast to P_{OUT} state observed during scanning *(Llacer et al 2015; Llacer et al 2021; Yi et al 2022; Petrychenko et al 2024)*. A distinct difference of 7.0Å could be seen by comparing the $tRNA_i$ position of EMCV IRES-48S PIC with that in the open state (Fig. 2B), depicting a P_{IN} state of $tRNA_i$. The entrapment of start codon in the P-site also evokes closure of the mRNA latch formed by 18S rRNA helices- h34 of 40S head and h18 of body (*Hussain et al 2014; Llacer et al 2015; Hinnebusch 2017*). The h34 of 18S rRNA of EMCV IRES-48S PIC is shifted by 9Å as compared to the human canonical open state 48S PIC (PDB- 7QP6, *Yi et al 2022*). This conformation of 18S rRNA corelates well with that of closed 48S PIC (PDB- 7QP7, *Yi et al 2022*), suggesting EMCV IRES-48S PIC was captured in a closed state (Fig. 1C). This closed conformation locks the mRNA in the channel formed within 40S head and body. On the other hand, the conformation of 18S rRNA in Map A (40S ribosome without initiation factors) shows an open state (Sup. Fig. 2E). The transition from open (PDB Id- 7QP6) to closed states (PDB Id- 7QP7) structures is also accompanied by an upward shift of N terminal domain of eS17 (connecting the head to body) by 10Å (*Yi et al 2022*). The EMCV IRES-48S PIC structure corelates with the conformation of eS17 in the human 48S-closed PIC, that is eS17 N-terminal helix associated with the ribosomal head shifts upward by 10Å, keeping C-terminal domain position constant (Fig. 2D; Sup. Fig. 2F).

Figure 2

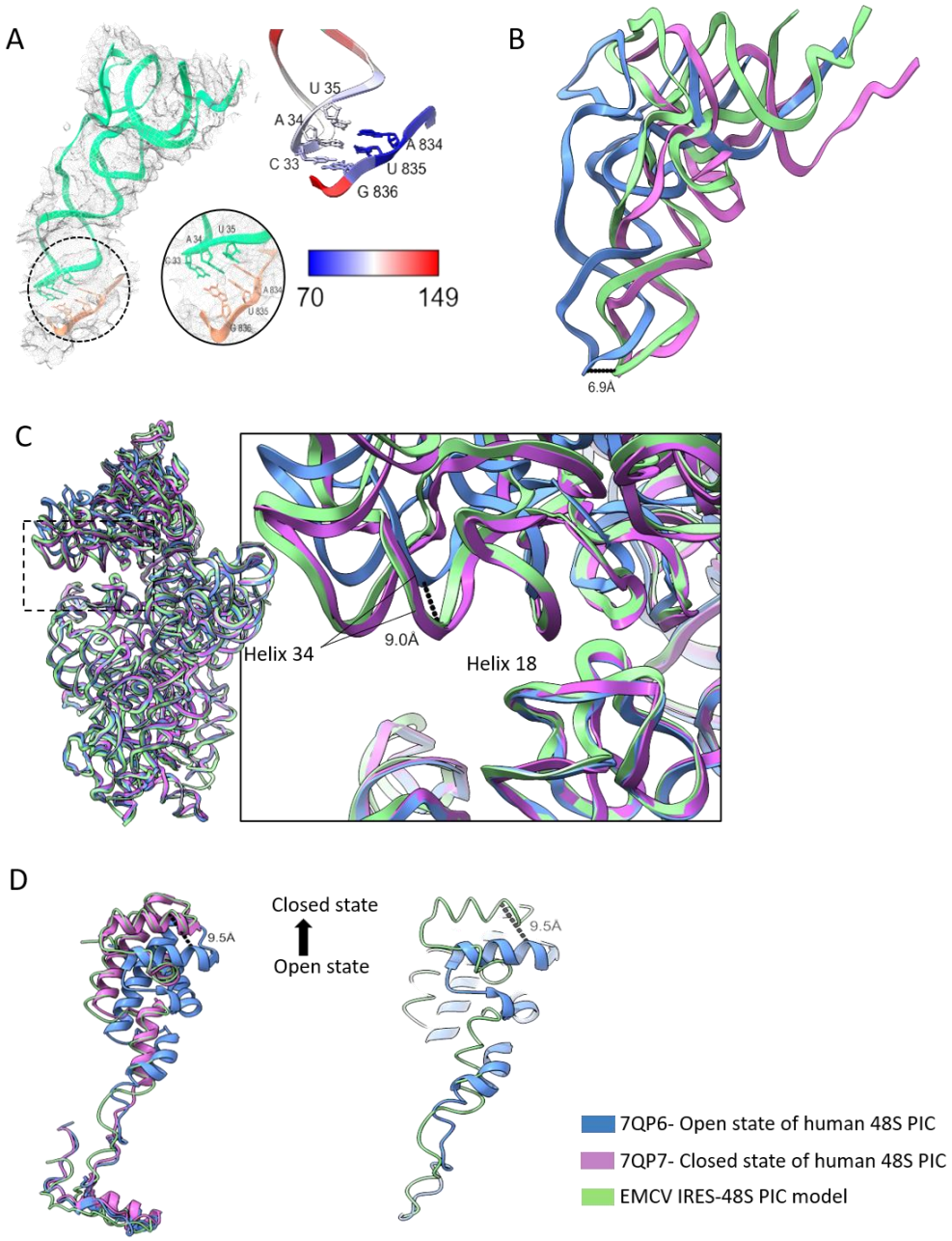

Figure 2 (A) Fitting of $tRNA_i$-base paired to start codon AUG (left). Zoomed view of codon-anticodon interaction (middle), and B-factor for codon-anticodon interaction (right). **(B)** The $tRNA_i$ in EMCV IRES-48S PIC is in P_{IN} state similar to that in human 48S PIC P_{IN} state (PDB Id- 7QP7) and its anticodon shows ~7 Å shift as compared to human 48S PIC open state (PDB Id- 7QP6). **(C)** Comparison of ribosomal conformation (18S rRNA) of EMCV IRES 48S PIC with Human open and closed state (PDB Id- 7QP6 and 7QP7, respectively). Focusing on the entry site and the helices governing latch conformation- Helix 34 moves toward helix 18 by 9 Å. **(D)** Movement of eS17 in open and closed states of ribosome. Zoomed view of comparison between eS17 in EMCV IRES 48S PIC and Human 48S PIC open state- showing an upward shift of the N terminal domain by 10Å.

3. The IRES density connecting 40S head to $tRNA_i$ is contributed by the I domain apical part

In EMCV IRES-48S PIC complex we observed a density, likely for double stranded RNA, connecting 40S head to the $tRNA_i$ elbow region (Fig. 3A). The extra density interacts with the elbow region and acceptor stem of $tRNA_i$ and ribosomal proteins- uS19 (RPS15) and uS13 (RPS18) *(Nomenclature- Ban et al 2014)*. The EMCV IRES contains 4 major stem-loops (H-L) in the functional IRES region (Fig. 3B) *(Hellen and Wimmer 1995)*. Among these, domain H and I have been shown to interact with 40S *(Chamond et al 2014)* and mutations of conserved residues in these domains severely compromised translation on EMCV IRES *(López de Quinto and Martínez-Salas 1997; Hellen and Wimmer 1995)*. We reasoned that H and I domain may contribute to the double stranded RNA density emanating from 40S head. The density architecture (Fig. 3C) could be interpreted as a long main stem (S1) extending away from 40S where the base is anchored to the ribosome by two branches (B1 and B2), and to $tRNA_i$ by one branch (B3), further divided into two sub-branches (B3a and B3b). Visualizing the IRES RNAfold determined-secondary structure (Fig. 3D- which corelates with the experimental structure proposed in *Duke et al 1992*), this architecture could be contributed by the apical part of I domain.

To determine the tertiary structure of the I domain apex, the IRES region from nucleotide 507-619 was modelled using Alphafold3 (Sup. Fig. 3A). The model was decomposed and reconstructed based on the best-fit in the obtained density for the IRES using Chimera and Coot (Sup. Fig. 3A). The final model was generated after multiple rounds of geometry correction and real space refinements (Fig. 3E). The final model holds a correlation coefficient of 0.8 with respect to the map (Sup. Fig. 3B), where B1 is AAG loop, B2 is CAAA loop, B3a- GCGA loop, B3b- C rich loop1, and S1 is the major double stranded stem of I domain. The B-factor of the modelled IRES largely ranges from 124 to 200 (Sup. Fig. 3C). The Alphafold3 predicted model of H domain could not fit properly in the density (Sup. Fig. 3D). The J-K domain adopts a Y-shaped structure and its placement of its Cryo-EM (PDB Id- 8HUJ) or NMR (PDB Id- 2NBX) structure in the density would clash with 40S (Sup. Fig. 3E). Moreover, in context to EMCV IRES-48S PIC, J-K domain binds eIF4G and the location of eIF4G has been mapped close to ES6 of 18S rRNA, located near the left foot 40S ribosome (*Yu et al 2011*). The I domain apex model in EMCV IRES-48S PIC shows the RAAA and AAG motif contacts uS19 and

uS13, and the GNRA loop with $tRNA_i$ (Fig. 4A). These interactions with 40S head and $tRNA_i$ could be facilitated by the long length and flexible nature of I domain.

Figure 3

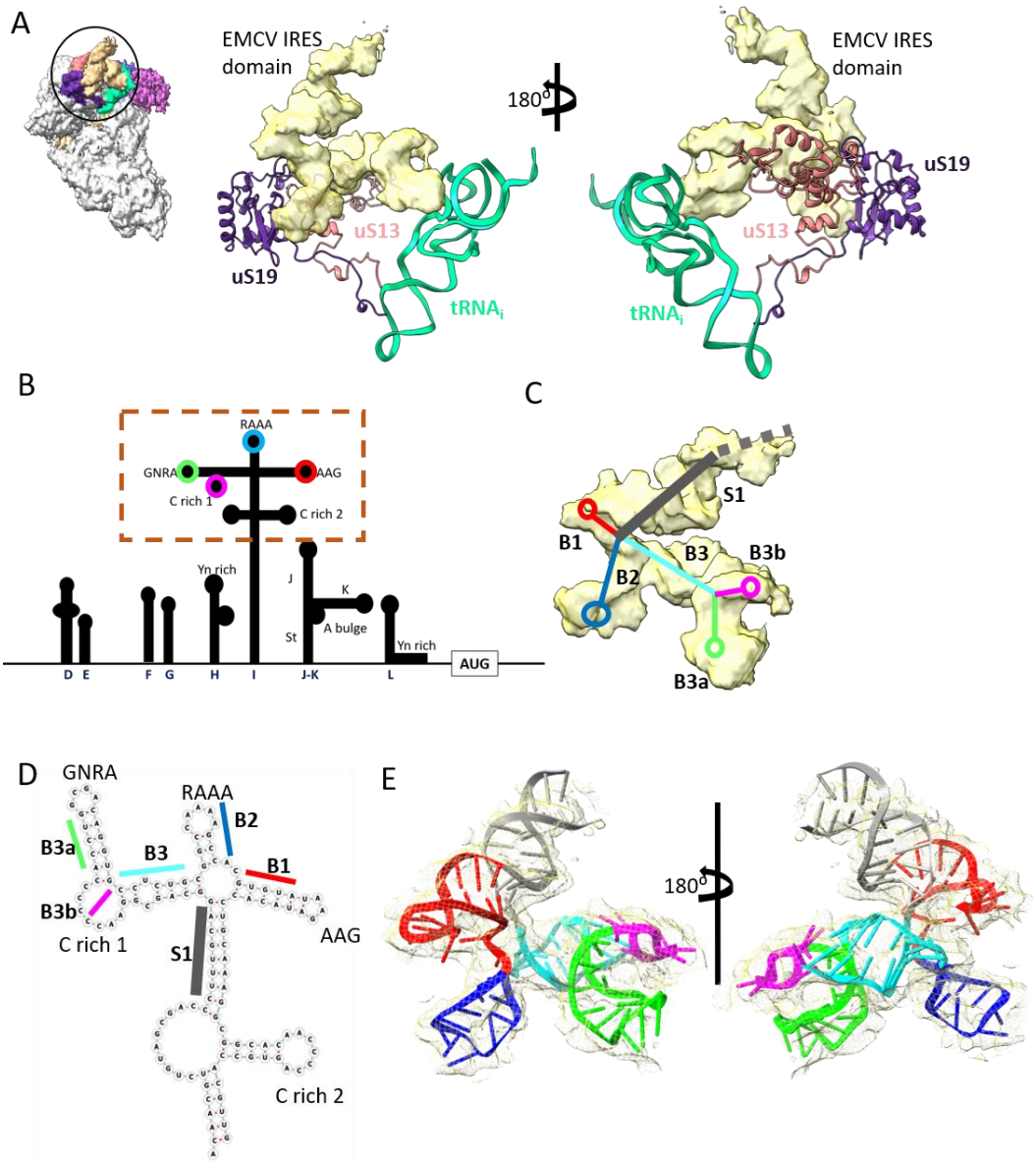

Figure 3 (A) Extra density connecting the head of 40S to $tRNA_i$ elbow region is contributed by EMCV IRES RNA in Map B1. Rotated views of RNA density showing its connection to the 40S head via uS13 and uS19 and to $tRNA_i$ via its elbow region. **(B)** Organization of EMCV IRES domains from D-L, where H-L makes the functional IRES moiety (*Hellen and Wimmer et al 1995*). **(C)** Deciphering the architecture of the obtained IRES density. The density could be interpreted as a long main stem (S1) extending away from the ribosome where the base is anchored to the ribosome by two branches (B1 and B2), and to $tRNA_i$ by one branch (B3), further divided into two sub-branches (B3a and B3b). **(D)** Secondary structure of apical region of domain I (made using RNAfold) marking the Stem and branches, along with imported loops. **(E)** Fitting of I domain apex in the density (Rotated views). The sub-domains are coloured as proposed in Fig 3C-D.

4. The interaction of I domain of EMCV IRES with ribosomal proteins and initiator tRNA

The I domain is the longest domain in EMCV IRES, which harbours important motifs such as GNRA, RAAA and C rich, crucial for IRES activity (*Roberts and Belsham, 1997; Fernández-Miragall and Martínez-Salas 2003*) and conserved across all cardioviruses (*Hellen and Wimmer 1995).* Among these, the CAAA and AAG motifs shares potential contact sites with uS13 and uS19. The alpha helix (100-117 residues) of uS13 contacts the IRES element at the B3 stem (connecting the GNRA loop to RAAA loop) (Fig. 4B). uS19 contacts the IRES majorly at its CAAA motif through multiple sites involving N-terminal residues, residues-67 to 75, C-terminal-102 to 124 (Fig. 4C). These regions of uS13 and uS19 is rich in basic residues, which might interact with the negatively charged backbone of the IRES element (Fig. 4B-C). The role of uS13 and uS19 also involves formation of inter-subunit bridges during 60S joining to form elongation competent 80S complexes. uS13 interacts with uL5 (RPL11) and uS19 with helix 38 or h38 (1748- 1778, in humans) in 28S rRNA to form inter-subunit bridges- B1b/c and B1a, respectively (Sup. Fig. 4A) (*Ben-Shem et al 2011; Bowen et al 2015; Khatter et al 2015*). These interactions are dynamic owing to ribosomal subunit rotation and swivelling during 80S ribosomal translocation states (*Khatter et al 2015*).

On superimposition of 80S ribosomal structure to EMCV IRES-48S PIC model, the IRES density clashes with the position of uL5 and h38 of 28S rRNA (Sup. Fig. 4B), suggesting repositioning of IRES domain from 40S head during 48S to 80S transition. Interestingly, the h38 residues interacting with uS19 shares considerable similarity in sequence to I domain apex in the EMCV IRES (Fig. 4D), suggesting the I domain apex of EMCV IRES could mimic h38 (60S)-40S interaction (Fig. 4D). The similarity of h38 with the I domain residues provides additional support for annotation of I domain apex in the density.

The GCGA (GNRA motif- where N is any nucleotide and R is a purine) is known for long range RNA-RNA interactions, widespread in ribosomal RNA and in some catalytic RNAs. It forms a characteristic U-turn structure (*Fiore and Nesbitt 2013*) and interacts with minor grooves of helical RNA elements (Sup. Fig. 4C- *Reiter et al 2010*). A single point mutation within this tetraloop (GCGA to GCGC) severely reduced the IRES activity, suggesting its essential for IRES activity (*Roberts and Belsham, 1997; Fernández-Miragall and Martínez-Salas 2003*). The

density extending from the elbow region of $tRNA_i$ could fit in the characteristic U-turn, adopted by conventional GNRA motifs. In EMCV IRES, the GNRA motif is represented by GCGA loop, preceded by a C rich region and in close contact with the $tRNA_i$ elbow and acceptor stem (Fig. 4E). Thus, we infer that EMCV IRES interacts with $tRNA_i$ by virtue of its GCGA loop.

Figure 4

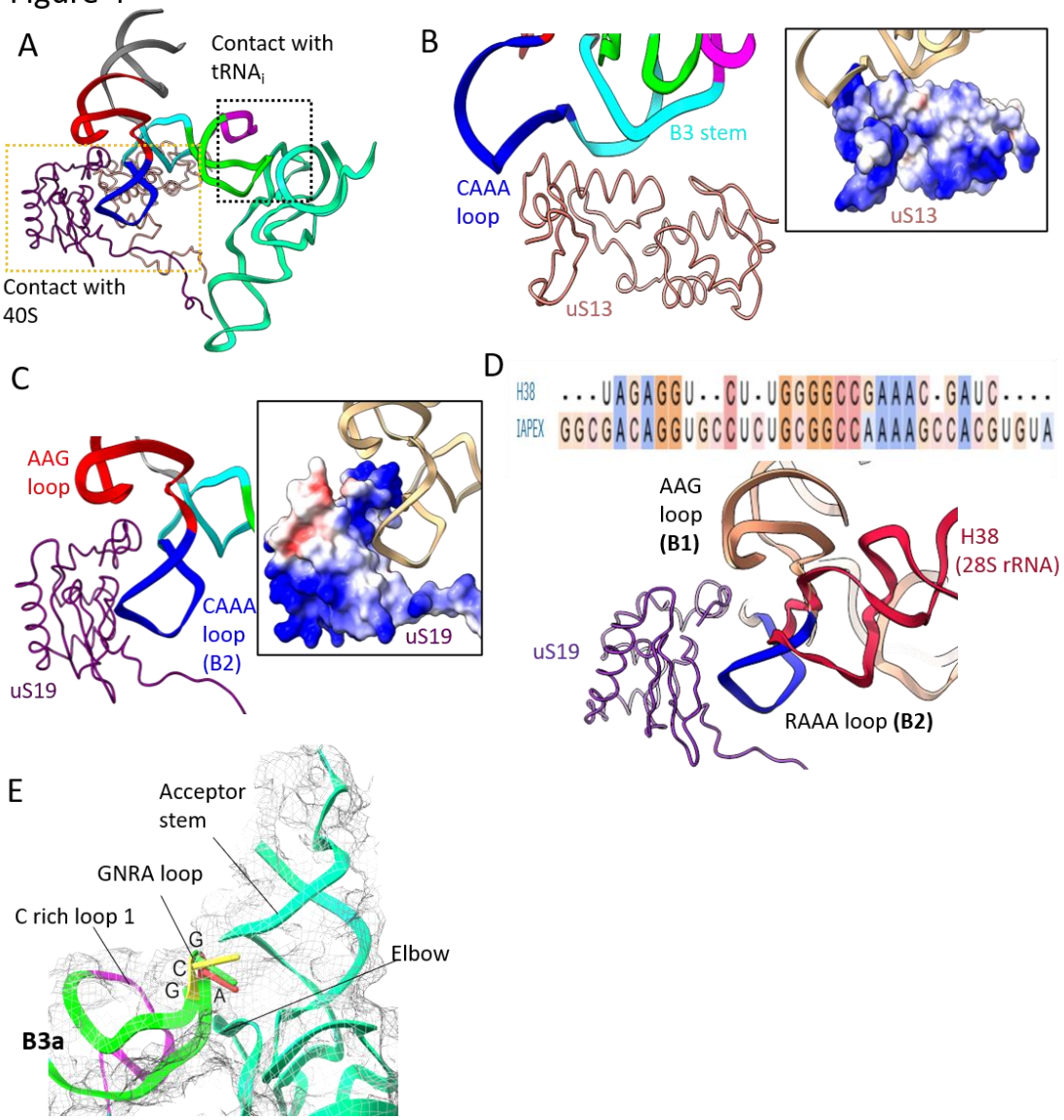

Figure 4 (A) Model showing connections of I domain apex with uS13, uS19, and $tRNA_i$. **(B)** uS13 interacts with B3 branch or sub-domain of IRES via its alpha helix (100-117 residues). **(C)** Multiple point of contacts between uS19 and I domain motifs- RAAA and AAG. The electrostatic potential map of uS19 suggests that EMCV IRES interacts via ionic interactions with its phosphate backbone. **(D)** Sequence alignment of h38 with I domain apex of EMCV IRES showing sequence identity. Overlapping of uS19 from 80S (PDB Id- 4UG0) and EMCV IRES-48S PIC show that the interaction of uS19 with EMCV IRES is similar to interaction with that of h38. **(E)** The fit of GNRA or GCGA stem and its contact with $tRNA_i$ at the elbow region and acceptor stem.

5. The position of eIF2-ternary complex is shifted towards 40S head in EMCV IRES-48S PIC in contrast to canonical 48S PIC

We could fit eIF2α and eIF2γ in their respective densities in Map B1 (Fig. 5A). Focussed classification or refinement did not yield any distinct density corresponding to the position of eIF2β, probably due to the flexibility associated with repositioning of eIF2β during transition from open to closed complexes *(Llacer et al 2015; Llacer et al 2021; Yi et al 2022; Petrychenko et al 2024)*. Previous reports on EMCV IRES suggested its direct interaction with eIF2 (*Scheper et al 1991; Scheper et al 1994*) and inactivation of eIF2 compromises EMCV IRES mediated translation *(*Welnowska *et al 2011; Kwon et al 2016)*, indicating EMCV IRES's dependence on canonical ternary complex. Here, we observe a direct interaction of EMCV IRES with ternary complex via $tRNA_i$, a feature not observed in previously determined HCV and CrPV IRESs-bound ribosomal structures.

As found in canonical 48S PICs (*Hashem et al 2013*; *Brito Querido et al 2024; Petrychenko et al 2024)*, eIF2α-domain 1 is in close contact with ribosomal protein- uS7, and domain 2 with $tRNA_i$ elbow and domain 3 with eIF2γ in EMCV IRES-48S PIC. The position of eIF2γ and eIF2α-domain3 (D3) is distinct from mammalian 48S-closed PICs (PDB Id- 6YAN and 7QP7) as we could observe a shift by ~10Å towards the head of 40S on superimposing the 18S rRNA from EMCV IRES 48S PIC and mammalian late-stage 48S PIC (Fig. 5B). The ternary complex is flexible, and it moves away from ribosomal head towards the body on recognition of authentic start codon as studied in yeast (*Villamayor-Belinchón et al 2024*) and human (*Petrychenko et al 2024)*. This opposite directional shift of the ternary complex in the EMCV IRES-48S PIC is evident in $tRNA_i$ acceptor stem as well (Fig. 5C). This shift could be due to the rigid stem B3 (consisting G-C base pairs), connecting 40S head to GNRA loop, which interacts with the $tRNA_i$ at its elbow and acceptor arm, and the association of eIF2α-D3 and eIF2γ with the acceptor arm of $tRNA_i$ orchestrated with the conformational change.

Figure 5

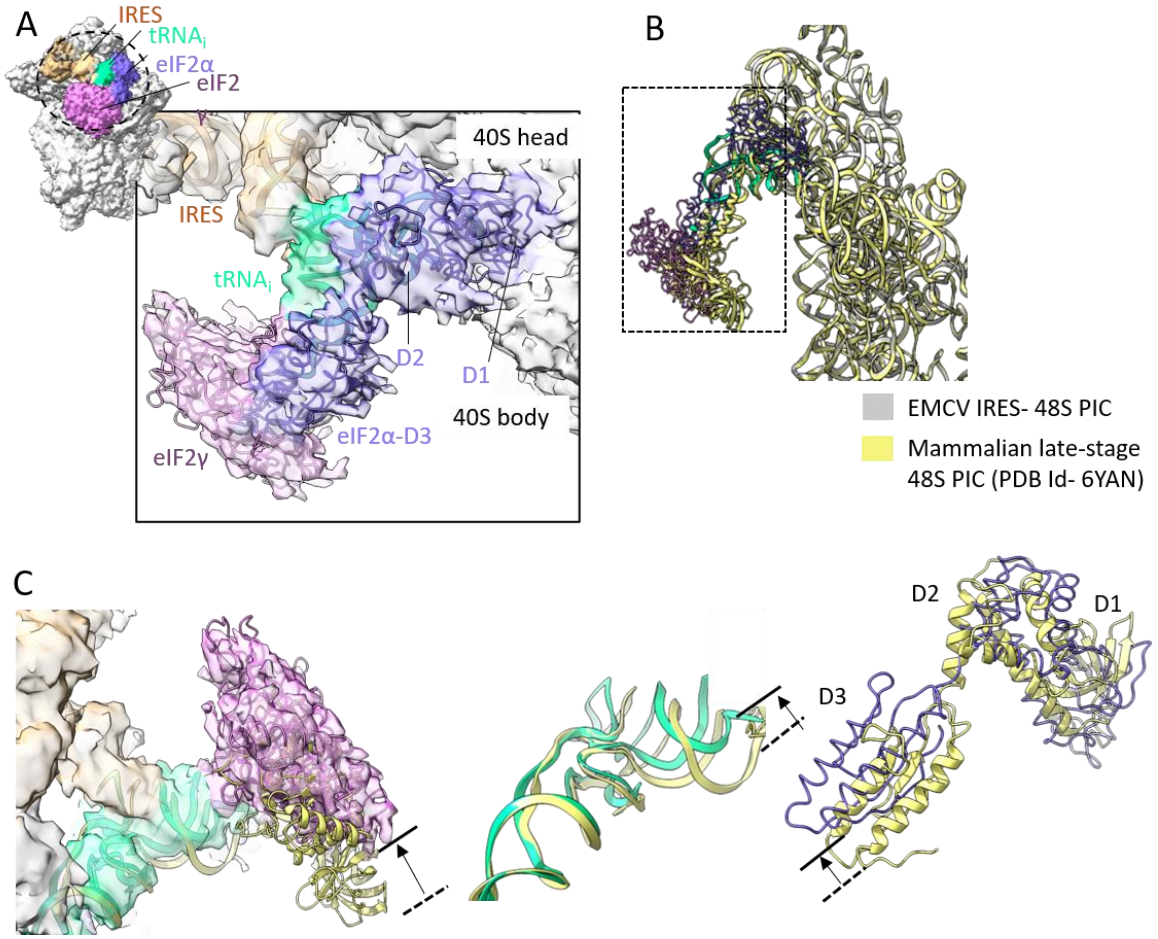

Figure 5 (A) Inter-subunit view of EMCV IRES 48S PIC showing position for ternary complex on map. Fitting of eIF2α and eIF2γ in its corresponding density in Map B1. **(B)** Overlapping EMCV IRES 48S PIC on mammalian late-stage 48S PIC (PDB Id- 6YAN), indicates a shift in position of eIF2γ towards 40S head. **(C)** Zoomed view showing position of eIF2γ, $tRNA_i$, eIF2α from EMCV IRES 48S PIC with respect to position on mammalian late-stage 48S PIC (PDB Id- 6YAN). The black arrow indicates the shift in position.

Discussion:

The mechanism of IRES recruitment on 40S ribosome varies considerably among different types of IRESs. CrPV intergenic IRES binds to 40S ribosome by mimicking tRNA-mRNA interaction with the help of pseudoknot 1 *(Petrov et al 2016; Fernandez et al 2014; Murray et al 2016; Acosta-Reyes et al 2019)*, whereas HCV IRESs associates with the solvent side of 40S body by replacing eIF3 with its domain 3 *(Spahn et al. 2004; Hashem et al 2013; Niepmann and Gerresheim 2020; Brown et al 2022)*. In this study, we capture EMCV IRES in 48S PIC

context, interacting with 40S ribosomal head and $tRNA_i$. Model building suggests that I domain of EMCV IRES interacts with 40S ribosome head and $tRNA_i$ elbow stem (Fig. 6A). The similarity in the sequence of h38 of 28S rRNA with the I domain and its ability to interact with uS19-N terminal via RAAA motif (*Khatter et al 2015*) suggests a mimicry mechanism adopted by EMCV IRES for its recruitment to the ribosome. Moreover, the conservation of I domain apex sequence and motifs (RAAA, AAG loop, C-rich and GNRA) across Cardioviruses- Theiler's murine Encephalitis virus (TMEV), Vilyuisk human encephalomyelitis virus (VHEV), Theiler's-like rat virus (TRV) and Saffold viruses 1 and 2 (SAFV-1 and SAFV-2) and Apthoviruses (AAG loop is replaced by ACG loop)- Foot and mouth disease virus (*Hellen and Wimmer 1995; Liang et al 2008*) suggests that these IRESs might adopt similar strategies for 48S formation (Fig. 6B-C). EMCV IRES can directly interact with 40S unlike type 1 IRESs. The I domain of EMCV IRES is similar to domain IV of polioviral IRES (or other type 1 IRESs) in terms of length, secondary structure and conserved motif's (GNRA, C-rich) positioning (Fig. 6C), therefore, anticipating a similar interaction with $tRNA_i$, highlighting a sequestering tendency by competing with cellular mRNAs. However, the lack of RAAA motif in type 1 provides a plausible reason for no direct interaction between type 1 IRES and 40S (*Lozano and Martinez-Salas 2015*).

The EMCV IRES does not require scanning, and the start codon (A-834) is directly placed in the P-site, which would eventually place the L domain at the mRNA exit site, preceded by J-K domain that interacts with eIF4G-eIF4A (Fig. 6A). Earlier, biochemical studies suggested eIF4G to be positioned close to ES6 of 18S rRNA in EMCV IRES-bound 48S PIC (*Yu et al 2011*). The human 48S PIC with a 5' capped mRNA showed a similar location for eIF4G, that is at the mRNA exit site contacting eIF3 (*Brito Querido et al 2020; Brito Querido et al 2024)*. Locating eIF4F have been challenging due to inherent flexibility associated with the eIF4F complex on mRNA and requires association with eIF3 in canonical 48S context (*Brito Querido et al 2020; Brito Querido et al 2024)*. However, eIF3-eIF4G interaction is dispensable for EMCV IRES-48S PIC formation, so we do not rule out the possibility that EMCV IRES may dislodge eIF3 from its position on the solvent surface as observed in case of HCV IRES (*Hashem et al 2013*). Although, PTB1 serves as an essential ITAF for 48S PIC formation on EMCV IRES, the obtained map shows no distinct density to PTB1. PTB1 binds to H domain and I domain base, and K domain loop (*Kafasla et al 2009*) and the flexibility associated with these domains might have hindered capturing of PTB1 in the reported 48S complex (Fig. 6A). However, the unassigned

extra density at the mRNA entry site could be contributed by PTB1-RRM interacting with 18S rRNA as discussed previously.

Figure 6

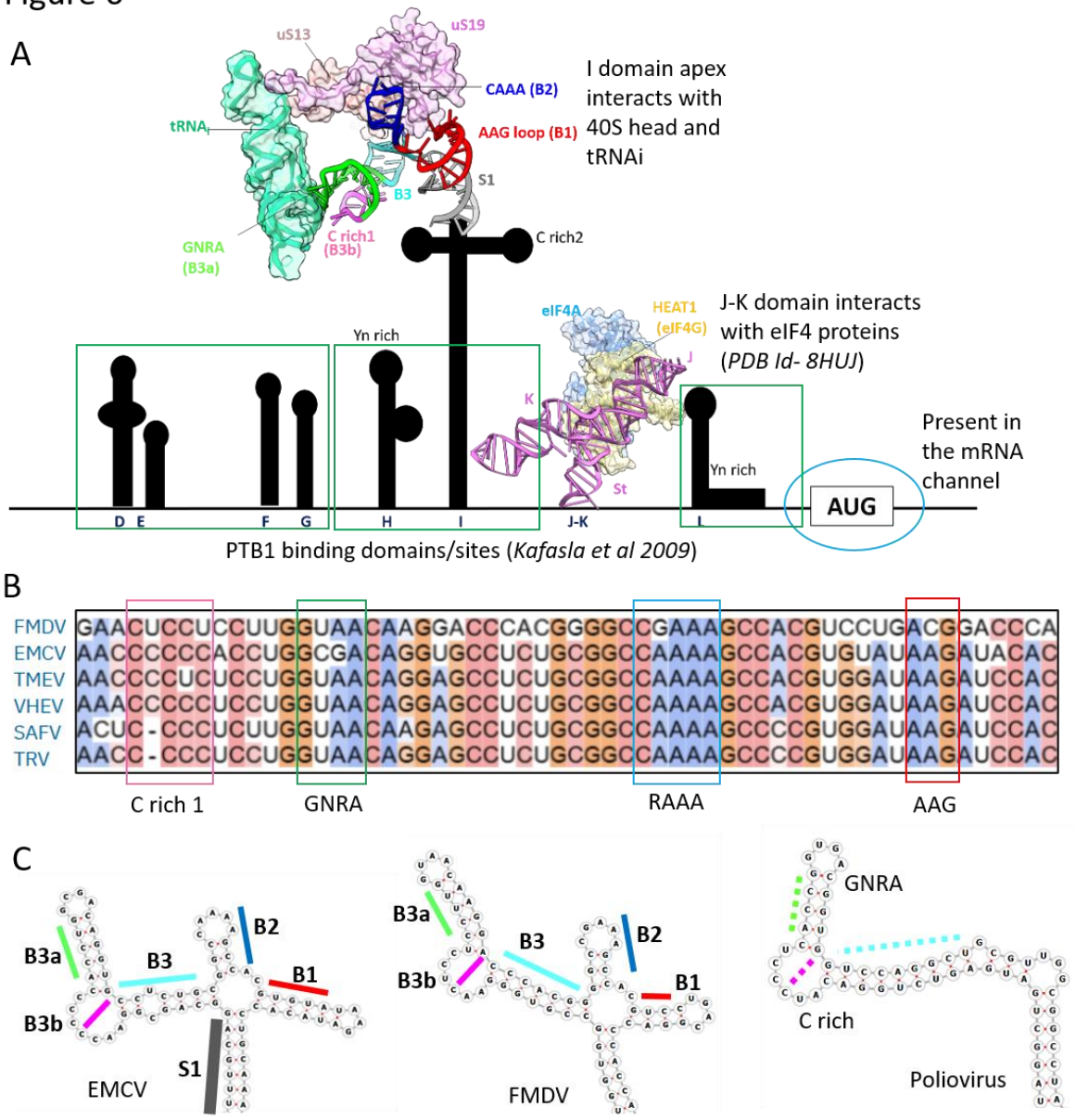

Figure 6 (A) EMCV IRES secondary structure depicting the role or binding partners for each domain in context to translation initiation. The known tertiary structure of EMCV IRES and its binding partners are depicted. The domains responsible for binding PTB1 are boxed. **(B)** Conservation of I domain apex sequence and secondary structure across type 2 IRES family. **(C)** Comparison of secondary structure of EMCV and FMDV IRES to that of Polioviral IRES (type 1).

The structural studies on type 2 IRESs have been limited be due to their flexible nature. In the cryo-EM map and structural analysis presented here, we could capture a part of EMCV IRES in 48S context (Fig. 6A) and fetch a significant understanding of ribosomal recruitment by EMCV IRES and 48S PIC formation. The entrapment of additional factors and a higher resolution would significantly provide more insights into EMCV IRES 48S PIC. The conservation of secondary structures and motifs such as GNRA within the picornaviruses (type 1, 2, and Aichiviral IRESs- *Abdullah et al 2023*) provokes common strategies of interaction in the context of 48S PICs in the Picornaviridae family.

Materials and Methods:

1. Plasmid constructs and Molecular Cloning

EMCV IRES 905 was obtained from EMCV-L plasmid- EMCV IRES (nt 280–905) into pCR2.1 and inserted in pcDNA3.1 using BamH1 and Xba1 restriction sites. Polypyrimidine tract binding protein 1 was cloned from HEK293 cDNA and 3C protease site (LEVLFQGP) was inserted at the N-terminal and inserted in pET28a in between BamH1 and HindIII restriction sites, retaining the N-terminal 6X Histidine tag. Sequence of oligos or primers used is listed in Sup. Table 1.

2. Protein overexpression and purification

PTB1 (Histidine tag- 3Cprotease site- PTB1 gene) was overexpressed using 0.5mM IPTG in *E. coli* BL21 cells at 30°C, 120 rpm for 4 hours in Luria broth. 2l harvested culture was lysed using Buffer N1 (20 mM HEPES pH-7.4, 300 mM KCl, 2mM $MgCl_2$, 10 % Glycerol, 10mM Imidazole, 5mM β-Mercaptoethanol, 0.05% Triton-X-100, 2mM PMSF) and sonicated at 18% amplitude, 10s ON and 20s OFF pulses, 30 cycles and centrifuges at 20000 rpm for 20 minutes and the supernatant was loaded on Ni-NTA column and eluted using a gradient of N1 to N2 buffer (20 mM HEPES pH-7.4, 300 mM KCl, 2mM $MgCl_2$, 10 % Glycerol, 500mM Imidazole, 5mM β-Mercaptoethanol). PTB1 was eluted at 250 mM Imidazole concentration. The eluant fractions (diluted to 100 mM KCl) were further loaded on Heparin column and eluted by applying a gradient of 100 mM to 1000 mM KCl. The protein was eluted at 250 mM KCl concentration. The eluant fractions were stored at -80°C after Size Exclusion Chromatography in Buffer S (20 mM HEPES pH-7.4, 200 mM KCl, 2mM $MgCl_2$, 5 % Glycerol, 1mM DTT) at 2.5 mg/ml concentration.

3C protease was overexpressed using 0.5mM IPTG in *E. coli* BL21 cells at 30°C, 120 rpm in Luria broth. 2l harvested culture was lysed using Buffer N11 (20 mM HEPES pH-7.4, 200 mM KCl, 2mM $MgCl_2$, 10 % Glycerol, 10mM Imidazole, 5mM β-Mercaptoethanol, 0.05% Triton-X-100, 2mM PMSF) and sonicated at 18% amplitude, 10s ON and 20s OFF pulses, 30 cycles and centrifuges at 20000 rpm for 20 minutes and the supernatant was loaded on Ni-NTA column and eluted using a gradient of N11 to N22 buffer (20 mM HEPES pH-7.4, 200 mM KCl, 2mM $MgCl_2$, 10 % Glycerol, 500mM Imidazole, 5mM β-Mercaptoethanol). 3C protease was eluted at 250 mM Imidazole concentration. The eluant fractions were subjected to Size Exclusion Chromatography in Buffer S (20 mM HEPES pH-7.4, 100 mM KOAc, 2mM $MgCl_2$, 10 % Glycerol, 1mM DTT) and peak fractions were concentrated using 3kDa cutoff centricon and stored at 2.5 mg/ml concentration.

3. In vitro transcription of EMCV IRES

EMCV IRES 905-pcDNA3.1 was linearized using Xba1 restriction enzyme and transcribed using Promega-RiboMAX™ Large Scale RNA Production Systems as per manufacturer's protocol. 1 µg of linearized plasmid yielded 87 µg of RNA after DNase treatment and RNA cleanup (RNA clean up kit- NEB).

4. Assembly of EMCV IRES 48S PIC using Talon Affinity Chromatography

12 µg of IRES was heated at 95°C to dissolve any secondary structures acquired and refolded using Buffer R (20 mM HEPES pH-7.4, 150 mM KOAc, 2mM $MgCl_2$, 2mM β-Mercaptoethanol, 0.5mM Spermidine) at 37°C for 5 mins and PTB1 (1:2 = IRES: PTB1) is added and further incubated at 30°C for 5 mins. Simultaneously, Rabbit Reticulocyte Lysate (RRL) (Promega) was incubated at 30°C with ATP, Amino acid mix minus Leucine, Murine RNase Inhibitor for 5 minutes and then mixed with IRES-PTB1 vial with instant addition of 6mM GMP-PnP per reaction (100 µl) and incubated at 30°C for 8 minutes, followed by ice incubation. The reaction was loaded on Talon beads equilibrated with Buffer A (20 mM HEPES pH-7.4, 150 mM KOAc, 2mM $MgCl_2$, 4 % Glycerol, 5mM Imidazole, 2mM β-Mercaptoethanol). After recommended passes, reloading and incubation, the flow through was collected and the beads were washed with Buffer A until A260 attains a baseline value (~0), following which 3C protease in Buffer A was added to the beads and left for overnight incubation. Fractions were eluted using Buffer A (400 µl each in 10 vials) and subjected to analysis such as A260 measurements, and agarose

gel electrophoresis. Samples having the RNA bands were pelleted using an 1ml Sucrose cushion (20 mM HEPES pH-7.4, 150 mM KOAc, 2mM $MgCl_2$, 30% Sucrose, 1mM DTT) in SW60 tubes and centrifuged at 50,000 rpm for 10 hours at 4°C. The pellet was resuspended in 20µl buffer R (+0.2 mM Spermidine) and used for Cryo-EM grid preparation (No crosslinker was used to avoid artifacts).

5. Negative stain analysis and Mass Spectrometry

Final sample was diluted 10 times using Buffer R and applied on 400-mesh Cu TEM grids which were freshly glow-discharged (negative polarity) for 30 s in GloQube glow-discharge system, stained using 1% Uranyl acetate solution and analysed using microscope at 57000 X magnification. Furthermore, the sample was digested by trypsin and subjected to NanoOrbitrap analysis for identification of proteins in the complex.

6. Cryo-EM sample preparation

3 µl of resuspended pellet (2.96 A260) was applied on glow discharged Quantifoil R 1.2/1.3 300 mesh 2nm Carbon Coated Grid and Blotted using 8s and 8.5s Blot time, zero Blot force at 16°C and 100% Humidity and plunged into liquid ethane. Cryo-EM data were collected on Talos Arctica transmission electron microscope equipped with a FEG at 200 kV (Thermo Fisher Scientific). All data were collected using a Gatan K2 Summit Direct Detector at a nominal magnification of 36,000 X and a pixel size of 1.17 Å with a total electron dose of 55 e- /Å2 fractionated over 20 frame movies with a dose rate of ~2.5 e-/Å^2 /frame.

6. Data Processing

Micrographs were collected and processed using CryoSPARC v3.3 (*Punjani et al 2017*). The micrographs were patch motion corrected and CTF was estimated. Using a blob picker with an average diameter of 300 Å particles were picked and extracted. The extracted particles were subjected to multiple rounds of 2D classification. Final 2D classes showing promising ribosome 2D features were selected for *ab initio* reconstruction. The junk was discarded, and the 237054 good particles were classified into 2 classes using a mask around $tRNA_i$. We obtained 2 classes- Empty 40S (1.25L particles- Class 1 or Map A), and 40S with tRNA bound (1.11L particles- Class 2). Class 2 was further classified into 2 classes using a 3D mask around the IRES density and subjected to non-uniform refinement with global CTF refinement to yield

Map B, having $tRNA_i$ and IRES density (55k particles). This was subjected to Non-uniform Refinement (*Punjani et al 2020*) with global CTF refinement. Map B class was further classified using a mask around eIF2α and eIF2γ to yield 2 classes- 40S-$tRNA_i$-IRES-eIF2 (28k particles- Map B1) and 40S-$tRNA_i$-IRES (26k particles). The obtained maps were then subjected to model building and refinement. The local resolution for the obtained maps were estimated using Phenix (*Liebschner et al 2019).*

7. Map analysis and Model building

To the obtained maps, 40S ribosome (PDB Id- 6YAN) was fitted using UCSF Chimera. The 40S head (Head proteins + 18S rRNA (1197-1688) + eS17) and 40S body (Body proteins + 18S rRNA (1-1196; 1689-1870)) was fitted to the obtained maps separately and subjected to Rigid Body Fit and Real Space Refinement using PHENIX *(Liebschner et al 2019)*. The models were merged using Coot *(Emsley et al 2010)* and subjected to Real Space Refinement. $tRNA_i$ and mRNA models were taken from PDB Id- 8OZ0 and fitted to the maps- B and B1 in Chimera. eIF2α and eIF2γ from PDB Id- 8OZ0 were rigid-body fitted to Map B1 and then mutated as per Rabbit eIF2 protein sequence (NCBI Reference Sequence- XP_002719561.1; XP_051683593.1) and subjected to a final Real Space Refinement. The IRES I domain apex model was predicted from Alphafold3 (*Abramson et al 2024*) and the helical sub-domains were dismantled and fitted according to best fit using Chimera, followed by chain joining in Coot with manual Real Space Refinement (*Afonine et al 2018*). The geometry was corrected using Geometry minimization tool in Phenix with rounds of Real Space Refinement. H domain model was predicted using Alphafold3. The final model yielded 40S-EMCV IRES-$tRNA_i$ (Map B) and 40S-EMCV IRES-$tRNA_i$-eIF2αϒ (Map B1). All the figures were made using ChimeraX *(Pettersen et al 2021).* The models were real space refined using Phenix and the Fourier Shell Correlation for 'Map to Model' for each was determined at 0.5 FSC (Sup. Fig. 2A-C; Table 1).

8. Secondary Structure Determination and Multiple sequence alignments

The secondary structures for I domain apex was obtained from RNAfold (*Gruber et al 2008*). Multiple sequence alignments were performed using Clustal Omega (*Sievers et al 2021*). Sequence accession number for various sequence used- EMCV (NC_001479.1), FMDV (NC_039210.1), TMEV (DQ401688.1), TRV (AB090161.1), VHEV (M80888.1), SAFV (FM207487.1), Poliovirus (NC_002058.3).

Accession codes:

Maps and atomic coordinates of the 40S ribosome (Map A), 40S ribosome-EMCV IRES-$tRNA_i$ (Map B) and 40S ribosome-EMCV IRES-ternary complex (Map B1) have been deposited in the EMDB database with accession codes- EMD-XXX, EMD-XXX, and EMD-XXX, respectively and in the PDB database with accession code XXX, XXX, and XXX, respectively.

Acknowledgements:

EMCV IRES (nt 280–905) into pCR2.1 was a kind gift from Dr. Bruno Sargueil, CNRS UMR8015, Universit ´e Paris Descartes, France and 3C protease-pET24 was a kind gift from Prof. Raghavan Varadarajan, Indian Institute of Science (IISc), India. We thank various central facilities, namely Cryo-EM, Mass Spectrometry and Computational cluster at the Division of Biological Sciences, IISc for support. DD acknowledges the DBT-JRF Programme for fellowship. The authors acknowledge the DST-FIST support to the department. This work was supported by the Intermediate Fellowship from DBT-Welcome Trust India Alliance to TH (IA/I/17/2/503313).

Conflict of Interest:

The authors declare no conflict of interest

References:

Abaeva IS, Young C, Warsaba R, Khan N, Tran LV, Jan E, Pestova TV, Hellen CUT. The structure and mechanism of action of a distinct class of dicistrovirus intergenic region IRESs. Nucleic Acids Res. 2023 Sep 22;51(17):9294-9313. doi: 10.1093/nar/gkad569. PMID: 37427788; PMCID: PMC10516663.

Abdullah SW, Wu J, Wang X, Guo H, Sun S. Advances and Breakthroughs in IRES-Directed Translation and Replication of Picornaviruses. mBio. 2023 Apr 25;14(2):e0035823. doi: 10.1128/mbio.00358-23. Epub 2023 Mar 20. PMID: 36939331; PMCID: PMC10127998.

Abramson J, Adler J, Dunger J, Evans R, Green T, Pritzel A, Ronneberger O, Willmore L, Ballard AJ, Bambrick J, Bodenstein SW, Evans DA, Hung CC, O'Neill M, Reiman D, Tunyasuvunakool K, Wu Z, Žemgulytė A, Arvaniti E, Beattie C, Bertolli O, Bridgland A, Cherepanov A, Congreve M, Cowen-Rivers AI, Cowie A, Figurnov M, Fuchs FB, Gladman H, Jain R, Khan YA, Low CMR, Perlin

K, Potapenko A, Savy P, Singh S, Stecula A, Thillaisundaram A, Tong C, Yakneen S, Zhong ED, Zielinski M, Žídek A, Bapst V, Kohli P, Jaderberg M, Hassabis D, Jumper JM. Accurate structure prediction of biomolecular interactions with AlphaFold 3. Nature. 2024 Jun;630(8016):493-500. doi: 10.1038/s41586-024-07487-w. Epub 2024 May 8. PMID: 38718835; PMCID: PMC11168924.

Acosta-Reyes F, Neupane R, Frank J, Fernández IS. The Israeli acute paralysis virus IRES captures host ribosomes by mimicking a ribosomal state with hybrid tRNAs. EMBO J. 2019 Oct 4;38(21):e102226. doi: 10.15252/embj.2019102226. Epub 2019 Oct 14. PMID: 31609474; PMCID: PMC6826211.

Afonine PV, Poon BK, Read RJ, Sobolev OV, Terwilliger TC, Urzhumtsev A, Adams PD. Real-space refinement in PHENIX for cryo-EM and crystallography. Acta Crystallogr D Struct Biol. 2018 Jun 1;74(Pt 6):531-544. doi: 10.1107/S2059798318006551. Epub 2018 May 30. PMID: 29872004; PMCID: PMC6096492.

Baglioni C, Simili M, Shafritz DA. Initiation activity of EMC virus RNA, binding to initiation factor eIF-4B and shut-off of host cell protein synthesis. Nature. 1978 Sep 21;275(5677):240-3. doi: 10.1038/275240a0. PMID: 211427.

Ban N, Beckmann R, Cate JH, Dinman JD, Dragon F, Ellis SR, Lafontaine DL, Lindahl L, Liljas A, Lipton JM, McAlear MA, Moore PB, Noller HF, Ortega J, Panse VG, Ramakrishnan V, Spahn CM, Steitz TA, Tchorzewski M, Tollervey D, Warren AJ, Williamson JR, Wilson D, Yonath A, Yusupov M. A new system for naming ribosomal proteins. Curr Opin Struct Biol. 2014 Feb;24:165-9. doi: 10.1016/j.sbi.2014.01.002. Epub 2014 Feb 10. PMID: 24524803; PMCID: PMC4358319.

Ben-Shem A, Garreau de Loubresse N, Melnikov S, Jenner L, Yusupova G, Yusupov M. The structure of the eukaryotic ribosome at 3.0 Å resolution. Science. 2011 Dec 16;334(6062):1524-9. doi: 10.1126/science.1212642. Epub 2011 Nov 17. PMID: 22096102.

Boehringer D, Thermann R, Ostareck-Lederer A, Lewis JD, Stark H. Structure of the hepatitis C virus IRES bound to the human 80S ribosome: remodeling of the HCV IRES. Structure. 2005 Nov;13(11):1695-706. doi: 10.1016/j.str.2005.08.008. PMID: 16271893.

Bowen AM, Musalgaonkar S, Moomau CA, Gulay SP, Mirvis M, Dinman JD. Ribosomal protein uS19 mutants reveal its role in coordinating ribosome structure and function. Translation (Austin). 2015 Nov 18;3(2):e1117703. doi: 10.1080/21690731.2015.1117703. PMID: 26824029; PMCID: PMC4721500.

Brito Querido J, Díaz-López I, Ramakrishnan V. The molecular basis of translation initiation and its regulation in eukaryotes. Nat Rev Mol Cell Biol. 2024 Mar;25(3):168-186. doi: 10.1038/s41580-023-00624-9. Epub 2023 Dec 5. PMID: 38052923.

Brito Querido J, Sokabe M, Díaz-López I, Gordiyenko Y, Fraser CS, Ramakrishnan V. The structure of a human translation initiation complex reveals two independent roles for the helicase eIF4A. Nat Struct Mol Biol. 2024 Mar;31(3):455-464. doi: 10.1038/s41594-023-01196-0. Epub 2024 Jan 29. PMID: 38287194; PMCID: PMC10948362.

Brito Querido J, Sokabe M, Kraatz S, Gordiyenko Y, Skehel JM, Fraser CS, Ramakrishnan V. Structure of a human 48*S* translational initiation complex. Science. 2020 Sep 4;369(6508):1220-1227. doi: 10.1126/science.aba4904. PMID: 32883864; PMCID: PMC7116333.

Brown ZP, Abaeva IS, De S, Hellen CUT, Pestova TV, Frank J. Molecular architecture of 40S translation initiation complexes on the hepatitis C virus IRES. EMBO J. 2022 Aug 16;41(16):e110581. doi: 10.15252/embj.2022110581. Epub 2022 Jul 13. PMID: 35822879; PMCID: PMC9379550.

Carocci M, Bakkali-Kassimi L. The encephalomyocarditis virus. Virulence. 2012 Jul 1;3(4):351-67. doi: 10.4161/viru.20573. Epub 2012 Jun 22. PMID: 22722247; PMCID: PMC3478238.

Chamond N, Deforges J, Ulryck N, Sargueil B. 40S recruitment in the absence of eIF4G/4A by EMCV IRES refines the model for translation initiation on the archetype of Type II IRESs. Nucleic Acids Res. 2014;42(16):10373-84. doi: 10.1093/nar/gku720. Epub 2014 Aug 26. PMID: 25159618; PMCID: PMC4176346.

Datey A, Sharma P, Khaja FT, Rahil H, Hussain T. Yeast Eukaryotic Initiation Factor 4B Remodels the MRNA Entry Site on the Small Ribosomal Subunit. Biochemistry. 2025 Feb 4;64(3):600-608. doi: 10.1021/acs.biochem.4c00489. Epub 2025 Jan 23. PMID: 39847343.

de Breyne S, Yu Y, Unbehaun A, Pestova TV, Hellen CU. Direct functional interaction of initiation factor eIF4G with type 1 internal ribosomal entry sites. Proc Natl Acad Sci U S A. 2009 Jun 9;106(23):9197-202. doi: 10.1073/pnas.0900153106. Epub 2009 May 22. PMID: 19470487; PMCID: PMC2695064.

des Georges A, Dhote V, Kuhn L, Hellen CU, Pestova TV, Frank J, Hashem Y. Structure of mammalian eIF3 in the context of the 43S preinitiation complex. Nature. 2015 Sep 24;525(7570):491-5. doi: 10.1038/nature14891. Epub 2015 Sep 7. PMID: 26344199; PMCID: PMC4719162.

Duke GM, Hoffman MA, Palmenberg AC. Sequence and structural elements that contribute to efficient encephalomyocarditis virus RNA translation. J Virol. 1992 Mar;66(3):1602-9. doi: 10.1128/JVI.66.3.1602-1609.1992. PMID: 1310768; PMCID: PMC240893.

Eliseev B, Yeramala L, Leitner A, Karuppasamy M, Raimondeau E, Huard K, Alkalaeva E, Aebersold R, Schaffitzel C. Structure of a human cap-dependent 48S translation pre-initiation complex. Nucleic Acids Res. 2018 Mar 16;46(5):2678-2689. doi: 10.1093/nar/gky054. PMID: 29401259; PMCID: PMC5861459.

Emsley P, Lohkamp B, Scott WG, Cowtan K. Features and development of Coot. Acta Crystallogr D Biol Crystallogr. 2010 Apr;66(Pt 4):486-501. doi: 10.1107/S0907444910007493. Epub 2010 Mar 24. PMID: 20383002; PMCID: PMC2852313.

Fernández IS, Bai XC, Murshudov G, Scheres SH, Ramakrishnan V. Initiation of translation by cricket paralysis virus IRES requires its translocation in the ribosome. Cell. 2014 May 8;157(4):823-31. doi: 10.1016/j.cell.2014.04.015. Epub 2014 May 1. PMID: 24792965; PMCID: PMC4017093.

Fernández N, Fernandez-Miragall O, Ramajo J, García-Sacristán A, Bellora N, Eyras E, Briones C, Martínez-Salas E. Structural basis for the biological relevance of the invariant apical stem in IRES-mediated translation. Nucleic Acids Res. 2011 Oct;39(19):8572-85. doi: 10.1093/nar/gkr560. Epub 2011 Jul 8. PMID: 21742761; PMCID: PMC3201876.

Fernández-Miragall O, López de Quinto S, Martínez-Salas E. Relevance of RNA structure for the activity of picornavirus IRES elements. Virus Res. 2009 Feb;139(2):172-82. doi: 10.1016/j.virusres.2008.07.009. Epub 2008 Aug 15. PMID: 18692097.

Fernández-Miragall O, Martínez-Salas E. Structural organization of a viral IRES depends on the integrity of the GNRA motif. RNA. 2003 Nov;9(11):1333-44. doi: 10.1261/rna.5950603. PMID: 14561883; PMCID: PMC1287055.

Fiore JL, Nesbitt DJ. An RNA folding motif: GNRA tetraloop-receptor interactions. Q Rev Biophys. 2013 Aug;46(3):223-64. doi: 10.1017/S0033583513000048. Epub 2013 Aug 5. PMID: 23915736.

Gruber AR, Lorenz R, Bernhart SH, Neuböck R, Hofacker IL. The Vienna RNA websuite. Nucleic Acids Res. 2008 Jul 1;36(Web Server issue):W70-4. doi: 10.1093/nar/gkn188. Epub 2008 Apr 19. PMID: 18424795; PMCID: PMC2447809.

Hashem Y, des Georges A, Dhote V, Langlois R, Liao HY, Grassucci RA, Pestova TV, Hellen CU, Frank J. Hepatitis-C-virus-like internal ribosome entry sites displace eIF3 to gain access to the 40S subunit. Nature. 2013 Nov 28;503(7477):539-43. doi: 10.1038/nature12658. Epub 2013 Nov 3. PMID: 24185006; PMCID: PMC4106463.

Hashem Y, des Georges A, Dhote V, Langlois R, Liao HY, Grassucci RA, Hellen CU, Pestova TV, Frank J. Structure of the mammalian ribosomal 43S preinitiation complex bound to the scanning factor DHX29. Cell. 2013 May 23;153(5):1108-19. doi: 10.1016/j.cell.2013.04.036. PMID: 23706745; PMCID: PMC3730827.

Hashem Y, des Georges A, Dhote V, Langlois R, Liao HY, Grassucci RA, Pestova TV, Hellen CU, Frank J. Hepatitis-C-virus-like internal ribosome entry sites displace eIF3 to gain access to the 40S subunit. Nature. 2013 Nov 28;503(7477):539-43. doi: 10.1038/nature12658. Epub 2013 Nov 3. PMID: 24185006; PMCID: PMC4106463.

Hellen CU, Wimmer E. Translation of encephalomyocarditis virus RNA by internal ribosomal entry. Curr Top Microbiol Immunol. 1995;203:31-63. doi: 10.1007/978-3-642-79663-0_2. PMID: 7555090.

Hinnebusch AG. Structural Insights into the Mechanism of Scanning and Start Codon Recognition in Eukaryotic Translation Initiation. Trends Biochem Sci. 2017 Aug;42(8):589-611. doi: 10.1016/j.tibs.2017.03.004. Epub 2017 Apr 22. PMID: 28442192.

Hussain T, Llácer JL, Fernández IS, Munoz A, Martin-Marcos P, Savva CG, Lorsch JR, Hinnebusch AG, Ramakrishnan V. Structural changes enable start codon recognition by the eukaryotic translation initiation complex. Cell. 2014 Oct 23;159(3):597-607. doi: 10.1016/j.cell.2014.10.001. Epub 2014 Oct 16. PMID: 25417110; PMCID: PMC4217140.

Imai S, Kumar P, Hellen CU, D'Souza VM, Wagner G. An accurately preorganized IRES RNA structure enables eIF4G capture for initiation of viral translation. Nat Struct Mol Biol. 2016 Sep;23(9):859-64. doi: 10.1038/nsmb.3280. Epub 2016 Aug 15. PMID: 27525590; PMCID: PMC5061125.

Imai S, Suzuki H, Fujiyoshi Y, Shimada I. Dynamically regulated two-site interaction of viral RNA to capture host translation initiation factor. Nat Commun. 2023 Aug 28;14(1):4977. doi: 10.1038/s41467-023-40582-6. PMID: 37640715; PMCID: PMC10462655.

International Committee on Taxonomy of Viruses Executive Committee. The new scope of virus taxonomy: partitioning the virosphere into 15 hierarchical ranks. Nat Microbiol. 2020 May;5(5):668-674. doi: 10.1038/s41564-020-0709-x. Epub 2020 Apr 27. PMID: 32341570; PMCID: PMC7186216.

Jackson RJ, Hellen CU, Pestova TV. The mechanism of eukaryotic translation initiation and principles of its regulation. Nat Rev Mol Cell Biol. 2010 Feb;11(2):113-27. doi: 10.1038/nrm2838. PMID: 20094052; PMCID: PMC4461372.

Jang SK, Kräusslich HG, Nicklin MJ, Duke GM, Palmenberg AC, Wimmer E. A segment of the 5' nontranslated region of encephalomyocarditis virus RNA directs internal entry of ribosomes during in vitro translation. J Virol. 1988 Aug;62(8):2636-43. doi: 10.1128/JVI.62.8.2636-2643.1988. PMID: 2839690; PMCID: PMC253694.

Johnson AG, Grosely R, Petrov AN, Puglisi JD. Dynamics of IRES-mediated translation. Philos Trans R Soc Lond B Biol Sci. 2017 Mar 19;372(1716):20160177. doi: 10.1098/rstb.2016.0177. PMID: 28138065; PMCID: PMC5311923.

Kafasla P, Morgner N, Pöyry TA, Curry S, Robinson CV, Jackson RJ. Polypyrimidine tract binding protein stabilizes the encephalomyocarditis virus IRES structure via binding multiple sites in a unique orientation. Mol Cell. 2009 Jun 12;34(5):556-68. doi: 10.1016/j.molcel.2009.04.015. PMID: 19524536.

Kafasla P, Morgner N, Robinson CV, Jackson RJ. Polypyrimidine tract-binding protein stimulates the poliovirus IRES by modulating eIF4G binding. EMBO J. 2010 Nov 3;29(21):3710-22. doi: 10.1038/emboj.2010.231. Epub 2010 Sep 21. PMID: 20859255; PMCID: PMC2982756.

Kaminski A, Belsham GJ, Jackson RJ. Translation of encephalomyocarditis virus RNA: parameters influencing the selection of the internal initiation site. EMBO J. 1994 Apr 1;13(7):1673-81. doi: 10.1002/j.1460-2075.1994.tb06431.x. PMID: 8157006; PMCID: PMC394998.

Khatter H, Myasnikov AG, Natchiar SK, Klaholz BP. Structure of the human 80S ribosome. Nature. 2015 Apr 30;520(7549):640-5. doi: 10.1038/nature14427. Epub 2015 Apr 22. PMID: 25901680.

Kolupaeva VG, Pestova TV, Hellen CU, Shatsky IN. Translation eukaryotic initiation factor 4G recognizes a specific structural element within the internal ribosome entry site of encephalomyocarditis virus RNA. J Biol Chem. 1998 Jul 17;273(29):18599-604. doi: 10.1074/jbc.273.29.18599. PMID: 9660832.

Kozak M. The scanning model for translation: an update. J Cell Biol. 1989 Feb;108(2):229-41. doi: 10.1083/jcb.108.2.229. PMID: 2645293; PMCID: PMC2115416.

Kwon OS, An S, Kim E, Yu J, Hong KY, Lee JS, Jang SK. An mRNA-specific tRNAi carrier eIF2A plays a pivotal role in cell proliferation under stress conditions: stress-resistant translation of c-Src mRNA is mediated by eIF2A. Nucleic Acids Res. 2017 Jan 9;45(1):296-310. doi: 10.1093/nar/gkw1117. Epub 2016 Nov 28. PMID: 27899592; PMCID: PMC5224483.

Lee KM, Chen CJ, Shih SR. Regulation Mechanisms of Viral IRES-Driven Translation. Trends Microbiol. 2017 Jul;25(7):546-561. doi: 10.1016/j.tim.2017.01.010. Epub 2017 Feb 24. PMID: 28242053.

Liang Z, Kumar AS, Jones MS, Knowles NJ, Lipton HL. Phylogenetic analysis of the species Theilovirus: emerging murine and human pathogens. J Virol. 2008 Dec;82(23):11545-54. doi: 10.1128/JVI.01160-08. Epub 2008 Sep 24. PMID: 18815294; PMCID: PMC2583687.

Liebschner D, Afonine PV, Baker ML, Bunkóczi G, Chen VB, Croll TI, Hintze B, Hung LW, Jain S, McCoy AJ, Moriarty NW, Oeffner RD, Poon BK, Prisant MG, Read RJ, Richardson JS, Richardson DC, Sammito MD, Sobolev OV, Stockwell DH, Terwilliger TC, Urzhumtsev AG, Videau LL, Williams CJ, Adams PD. Macromolecular structure determination using X-rays, neutrons and electrons: recent developments in Phenix. Acta Crystallogr D Struct Biol. 2019 Oct 1;75(Pt 10):861-877. doi: 10.1107/S2059798319011471. Epub 2019 Oct 2. PMID: 31588918; PMCID: PMC6778852.

Llácer JL, Hussain T, Marler L, Aitken CE, Thakur A, Lorsch JR, Hinnebusch AG, Ramakrishnan V. Conformational Differences between Open and Closed States of the Eukaryotic Translation Initiation Complex. Mol Cell. 2015 Aug 6;59(3):399-412. doi: 10.1016/j.molcel.2015.06.033. Epub 2015 Jul 23. PMID: 26212456; PMCID: PMC4534855.

Llácer JL, Hussain T, Dong J, Villamayor L, Gordiyenko Y, Hinnebusch AG. Large-scale movement of eIF3 domains during translation initiation modulate start codon selection. Nucleic Acids Res. 2021 Nov 18;49(20):11491-11511. doi: 10.1093/nar/gkab908. PMID: 34648019; PMCID: PMC8599844.

Lomakin IB, Hellen CU, Pestova TV. Physical association of eukaryotic initiation factor 4G (eIF4G) with eIF4A strongly enhances binding of eIF4G to the internal ribosomal entry site of encephalomyocarditis virus and is required for internal initiation of translation. Mol Cell Biol. 2000 Aug;20(16):6019-29. doi: 10.1128/mcb.20.16.6019-6029.2000. PMID: 10913184; PMCID: PMC86078.

López de Quinto S, Martínez-Salas E. Conserved structural motifs located in distal loops of aphthovirus internal ribosome entry site domain 3 are required for internal initiation of translation. J Virol. 1997 May;71(5):4171-5. doi: 10.1128/JVI.71.5.4171-4175.1997. PMID: 9094703; PMCID: PMC191578.

Lozano G, Martínez-Salas E. Structural insights into viral IRES-dependent translation mechanisms. Curr Opin Virol. 2015 Jun;12:113-20. doi: 10.1016/j.coviro.2015.04.008. Epub 2015 May 22. PMID: 26004307.

Maris C, Jayne S, Damberger FF, Beusch I, Dorn G, Ravindranathan S, Allain FH. A transient α-helix in the N-terminal RNA recognition motif of polypyrimidine tract binding protein senses RNA secondary structure. Nucleic Acids Res. 2020 May 7;48(8):4521-4537. doi: 10.1093/nar/gkaa155. PMID: 32170319; PMCID: PMC7192611.

Martinez-Salas E, Francisco-Velilla R, Fernandez-Chamorro J, Embarek AM. Insights into Structural and Mechanistic Features of Viral IRES Elements. Front Microbiol. 2018 Jan 4;8:2629. doi: 10.3389/fmicb.2017.02629. PMID: 29354113; PMCID: PMC5759354.

Martínez-Salas E, Francisco-Velilla R, Fernandez-Chamorro J, Lozano G, Diaz-Toledano R. Picornavirus IRES elements: RNA structure and host protein interactions. Virus Res. 2015 Aug 3;206:62-73. doi: 10.1016/j.virusres.2015.01.012. Epub 2015 Jan 21. PMID: 25617758

Muhs M, Hilal T, Mielke T, Skabkin MA, Sanbonmatsu KY, Pestova TV, Spahn CM. Cryo-EM of ribosomal 80S complexes with termination factors reveals the translocated cricket paralysis virus IRES. Mol Cell. 2015 Feb 5;57(3):422-32. doi: 10.1016/j.molcel.2014.12.016. Epub 2015 Jan 15. PMID: 25601755; PMCID: PMC4526138.

Murray J, Savva CG, Shin BS, Dever TE, Ramakrishnan V, Fernández IS. Structural characterization of ribosome recruitment and translocation by type IV IRES. Elife. 2016 May 9;5:e13567. doi: 10.7554/eLife.13567. PMID: 27159451; PMCID: PMC4861600.

Neupane R, Pisareva VP, Rodriguez CF, Pisarev AV, Fernández IS. A complex IRES at the 5'-UTR of a viral mRNA assembles a functional 48S complex via an uAUG intermediate. Elife. 2020 Apr 14;9:e54575. doi: 10.7554/eLife.54575. PMID: 32286223; PMCID: PMC7190351.

Niepmann M, Gerresheim GK. Hepatitis C Virus Translation Regulation. Int J Mol Sci. 2020 Mar 27;21(7):2328. doi: 10.3390/ijms21072328. PMID: 32230899; PMCID: PMC7178104.

Ochs K, Saleh L, Bassili G, Sonntag VH, Zeller A, Niepmann M. Interaction of translation initiation factor eIF4B with the poliovirus internal ribosome entry site. J Virol. 2002 Mar;76(5):2113-22. doi: 10.1128/jvi.76.5.2113-2122.2002. PMID: 11836388; PMCID: PMC135939.

Pelletier J, Sonenberg N. Internal initiation of translation of eukaryotic mRNA directed by a sequence derived from poliovirus RNA. Nature. 1988 Jul 28;334(6180):320-5. doi: 10.1038/334320a0. PMID: 2839775.

Pestova TV, Hellen CU, Shatsky IN. Canonical eukaryotic initiation factors determine initiation of translation by internal ribosomal entry. Mol Cell Biol. 1996 Dec;16(12):6859-69. doi: 10.1128/MCB.16.12.6859. PMID: 8943341; PMCID: PMC231689.

Petrov A, Grosely R, Chen J, O'Leary SE, Puglisi JD. Multiple Parallel Pathways of Translation Initiation on the CrPV IRES. Mol Cell. 2016 Apr 7;62(1):92-103. doi: 10.1016/j.molcel.2016.03.020. PMID: 27058789; PMCID: PMC4826567.

Petrychenko V, Yi SH, Liedtke D, Peng BZ, Rodnina MV, Fischer N. Structural basis for translational control by the human 48S initiation complex. Nat Struct Mol Biol. 2024 Sep 17. doi: 10.1038/s41594-024-01378-4. Epub ahead of print. PMID: 39289545.

Pettersen EF, Goddard TD, Huang CC, Couch GS, Greenblatt DM, Meng EC, Ferrin TE. UCSF Chimera--a visualization system for exploratory research and analysis. J Comput Chem. 2004 Oct;25(13):1605-12. doi: 10.1002/jcc.20084. PMID: 15264254.

Pettersen EF, Goddard TD, Huang CC, Meng EC, Couch GS, Croll TI, Morris JH, Ferrin TE. UCSF ChimeraX: Structure visualization for researchers, educators, and developers. Protein Sci. 2021 Jan;30(1):70-82. doi: 10.1002/pro.3943. Epub 2020 Oct 22. PMID: 32881101; PMCID: PMC7737788.

Punjani A, Rubinstein JL, Fleet DJ, Brubaker MA. cryoSPARC: algorithms for rapid unsupervised cryo-EM structure determination. Nat Methods. 2017 Mar;14(3):290-296. doi: 10.1038/nmeth.4169. Epub 2017 Feb 6. PMID: 28165473.

Punjani A, Zhang H, Fleet DJ. Non-uniform refinement: adaptive regularization improves single-particle cryo-EM reconstruction. Nat Methods. 2020 Dec;17(12):1214-1221. doi: 10.1038/s41592-020-00990-8. Epub 2020 Nov 30. PMID: 33257830.

Quade N, Boehringer D, Leibundgut M, van den Heuvel J, Ban N. Cryo-EM structure of Hepatitis C virus IRES bound to the human ribosome at 3.9-Å resolution. Nat Commun. 2015 Jul 8;6:7646. doi: 10.1038/ncomms8646. PMID: 26155016; PMCID: PMC4510694.

Reiter NJ, Osterman A, Torres-Larios A, Swinger KK, Pan T, Mondragón A. Structure of a bacterial ribonuclease P holoenzyme in complex with tRNA. Nature. 2010 Dec 9;468(7325):784-9. doi: 10.1038/nature09516. Epub 2010 Nov 14. PMID: 21076397; PMCID: PMC3058908.

Roberts LO, Belsham GJ. Complementation of defective picornavirus internal ribosome entry site (IRES) elements by the coexpression of fragments of the IRES. Virology. 1997 Jan 6;227(1):53-62. doi: 10.1006/viro.1996.8312. PMID: 9007058.

Robertson ME, Seamons RA, Belsham GJ. A selection system for functional internal ribosome entry site (IRES) elements: analysis of the requirement for a conserved GNRA tetraloop in the encephalomyocarditis virus IRES. RNA. 1999 Sep;5(9):1167-79. doi: 10.1017/s1355838299990301. PMID: 10496218; PMCID: PMC1369840.

Scheper GC, Thomas AA, Voorma HO. The 5' untranslated region of encephalomyocarditis virus contains a sequence for very efficient binding of eukaryotic initiation factor eIF-2/2B. Biochim Biophys Acta. 1991 Jun 13;1089(2):220-6. doi: 10.1016/0167-4781(91)90011-a. PMID: 1647211.

Scheper GC, Voorma HO, Thomas AA. Binding of eukaryotic initiation factor-2 and trans-acting factors to the 5' untranslated region of encephalomyocarditis virus RNA. Biochimie. 1994;76(8):801-9. doi: 10.1016/0300-9084(94)90084-1. PMID: 7893829.

Sievers F, Higgins DG. The Clustal Omega Multiple Alignment Package. Methods Mol Biol. 2021;2231:3-16. doi: 10.1007/978-1-0716-1036-7_1. PMID: 33289883.

Simonetti A, Guca E, Bochler A, Kuhn L, Hashem Y. Structural Insights into the Mammalian Late-Stage Initiation Complexes. Cell Rep. 2020 Apr 7;31(1):107497. doi: 10.1016/j.celrep.2020.03.061. PMID: 32268096; PMCID: PMC7166083.

Spahn CM, Jan E, Mulder A, Grassucci RA, Sarnow P, Frank J. Cryo-EM visualization of a viral internal ribosome entry site bound to human ribosomes: the IRES functions as an RNA-based translation factor. Cell. 2004 Aug 20;118(4):465-75. doi: 10.1016/j.cell.2004.08.001. PMID: 15315759.

Spahn CM, Kieft JS, Grassucci RA, Penczek PA, Zhou K, Doudna JA, Frank J. Hepatitis C virus IRES RNA-induced changes in the conformation of the 40s ribosomal subunit. Science. 2001 Mar 9;291(5510):1959-62. doi: 10.1126/science.1058409. PMID: 11239155.

Sweeney TR, Abaeva IS, Pestova TV, Hellen CU. The mechanism of translation initiation on Type 1 picornavirus IRESs. EMBO J. 2014 Jan 7;33(1):76-92. doi: 10.1002/embj.201386124. Epub 2013 Dec 15. PMID: 24357634; PMCID: PMC3990684.

Trono D, Pelletier J, Sonenberg N, Baltimore D. Translation in mammalian cells of a gene linked to the poliovirus 5' noncoding region. Science. 1988 Jul 22;241(4864):445-8. doi: 10.1126/science.2839901. PMID: 2839901.

Villa N, Do A, Hershey JW, Fraser CS. Human eukaryotic initiation factor 4G (eIF4G) protein binds to eIF3c, -d, and -e to promote mRNA recruitment to the ribosome. J Biol Chem. 2013 Nov 15;288(46):32932-40. doi: 10.1074/jbc.M113.517011. Epub 2013 Oct 3. PMID: 24092755; PMCID: PMC3829144.

Villamayor-Belinchón L, Sharma P, Gordiyenko Y, Llácer JL, Hussain T. Structural basis of AUC codon discrimination during translation initiation in yeast. Nucleic Acids Res. 2024 Oct 14;52(18):11317-11335. doi: 10.1093/nar/gkae737. PMID: 39193907; PMCID: PMC11472065.

Welnowska E, Sanz MA, Redondo N, Carrasco L. Translation of viral mRNA without active eIF2: the case of picornaviruses. PLoS One. 2011;6(7):e22230. doi: 10.1371/journal.pone.0022230. Epub 2011 Jul 14. PMID: 21779397; PMCID: PMC3136507.

Yamamoto H, Collier M, Loerke J, Ismer J, Schmidt A, Hilal T, Sprink T, Yamamoto K, Mielke T, Bürger J, Shaikh TR, Dabrowski M, Hildebrand PW, Scheerer P, Spahn CM. Molecular architecture of the ribosome-bound Hepatitis C Virus internal ribosomal entry site RNA. EMBO J. 2015 Dec 14;34(24):3042-58. doi: 10.15252/embj.201592469. Epub 2015 Nov 24. PMID: 26604301; PMCID: PMC4687786.

Yamamoto H, Unbehaun A, Loerke J, Behrmann E, Collier M, Bürger J, Mielke T, Spahn CM. Structure of the mammalian 80S initiation complex with initiation factor 5B on HCV-IRES RNA. Nat Struct Mol Biol. 2014 Aug;21(8):721-7. doi: 10.1038/nsmb.2859. Epub 2014 Jul 27. PMID: 25064512.

Yi SH, Petrychenko V, Schliep JE, Goyal A, Linden A, Chari A, Urlaub H, Stark H, Rodnina MV, Adio S, Fischer N. Conformational rearrangements upon start codon recognition in human 48S translation initiation complex. Nucleic Acids Res. 2022 May 20;50(9):5282-5298. doi: 10.1093/nar/gkac283. PMID: 35489072; PMCID: PMC9122606.

Yokoyama T, Machida K, Iwasaki W, Shigeta T, Nishimoto M, Takahashi M, Sakamoto A, Yonemochi M, Harada Y, Shigematsu H, Shirouzu M, Tadakuma H, Imataka H, Ito T. HCV IRES Captures an Actively Translating 80S Ribosome. Mol Cell. 2019 Jun 20;74(6):1205-1214.e8. doi: 10.1016/j.molcel.2019.04.022. Epub 2019 May 9. PMID: 31080011.

Yu Y, Abaeva IS, Marintchev A, Pestova TV, Hellen CU. Common conformational changes induced in type 2 picornavirus IRESs by cognate trans-acting factors. Nucleic Acids Res. 2011 Jun;39(11):4851-65. doi: 10.1093/nar/gkr045. Epub 2011 Feb 8. PMID: 21306989; PMCID: PMC3113573.

Zhao J, Li Y, Wang C, Zhang H, Zhang H, Jiang B, Guo X, Song X. IRESbase: A Comprehensive Database of Experimentally Validated Internal Ribosome Entry Sites. Genomics Proteomics Bioinformatics. 2020 Apr;18(2):129-139. doi: 10.1016/j.gpb.2020.03.001. Epub 2020 Jun 6. PMID: 32512182; PMCID: PMC7646085.

Supplementary Information

Structural insights into the recruitment of viral Type 2 IRES to ribosomal preinitiation complex for protein synthesis

Deepakash Das and Tanweer Hussain

Department of Developmental Biology and Genetics, Indian Institute of Science, Bengaluru, INDIA. PIN-560012

*Correspondence: hussain@iisc.ac.in

This file contains 4 supplementary figures, 1 supplementary table and legend for supplementary movie 1.

Supplementary Figure 1.1

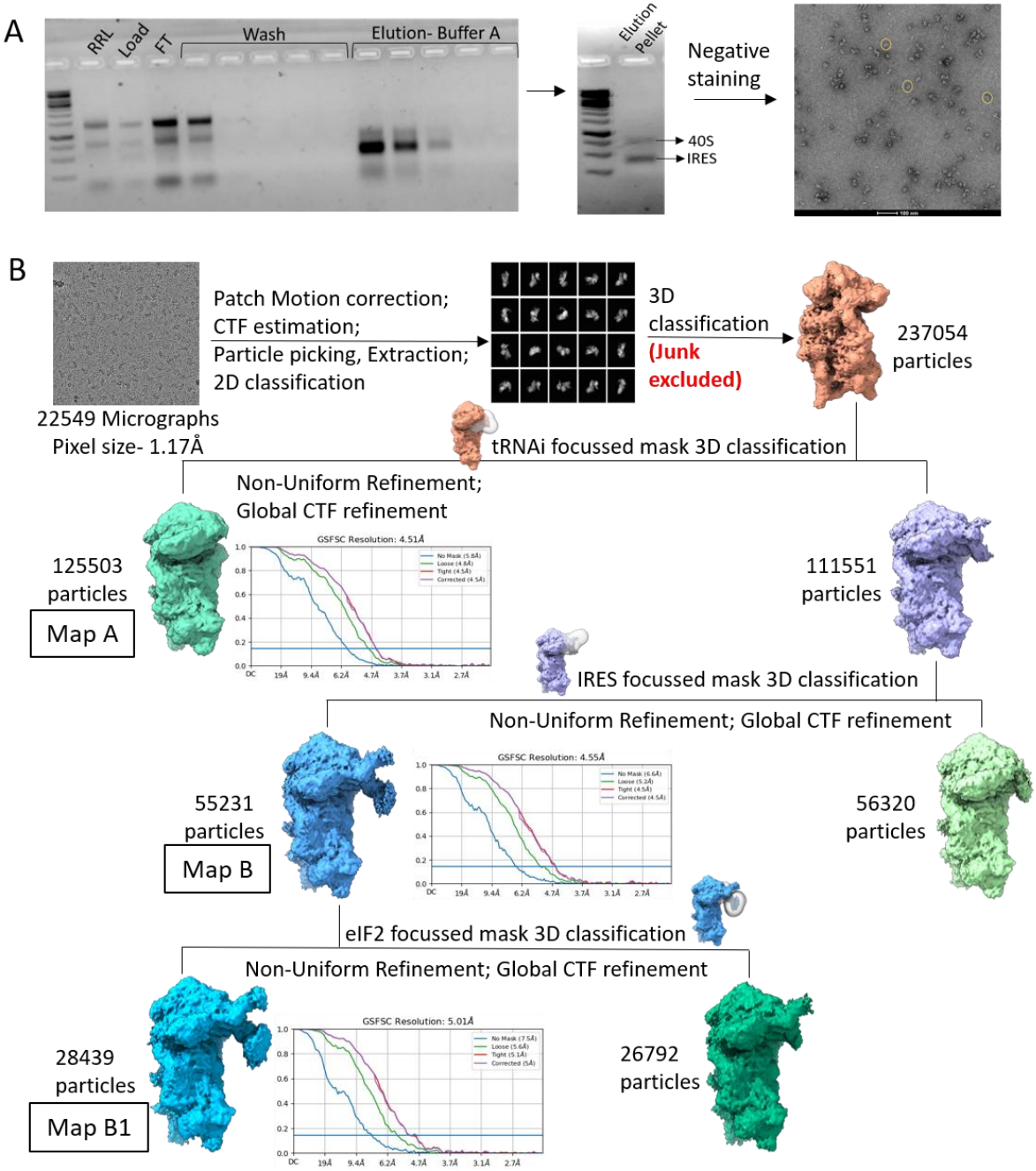

Supplementary Figure 1.1 (A) Isolation of EMCV IRES-48S PIC from Talon Affinity Chromatography- Talon Affinity chromatography profile and analysis of Elution fractions- pelleted by using 30% cushion on 1.5% Agarose gel, followed by Uranyl acetate staining of elution pellet and observation under transmission electron microscope at 57k X. **(B)** Processing of Cryo-EM data and features of obtained maps using CryoSPARCv4.3.0 and GSFSC resolution estimates for different maps obtained.

Supplementary Figure 1.2

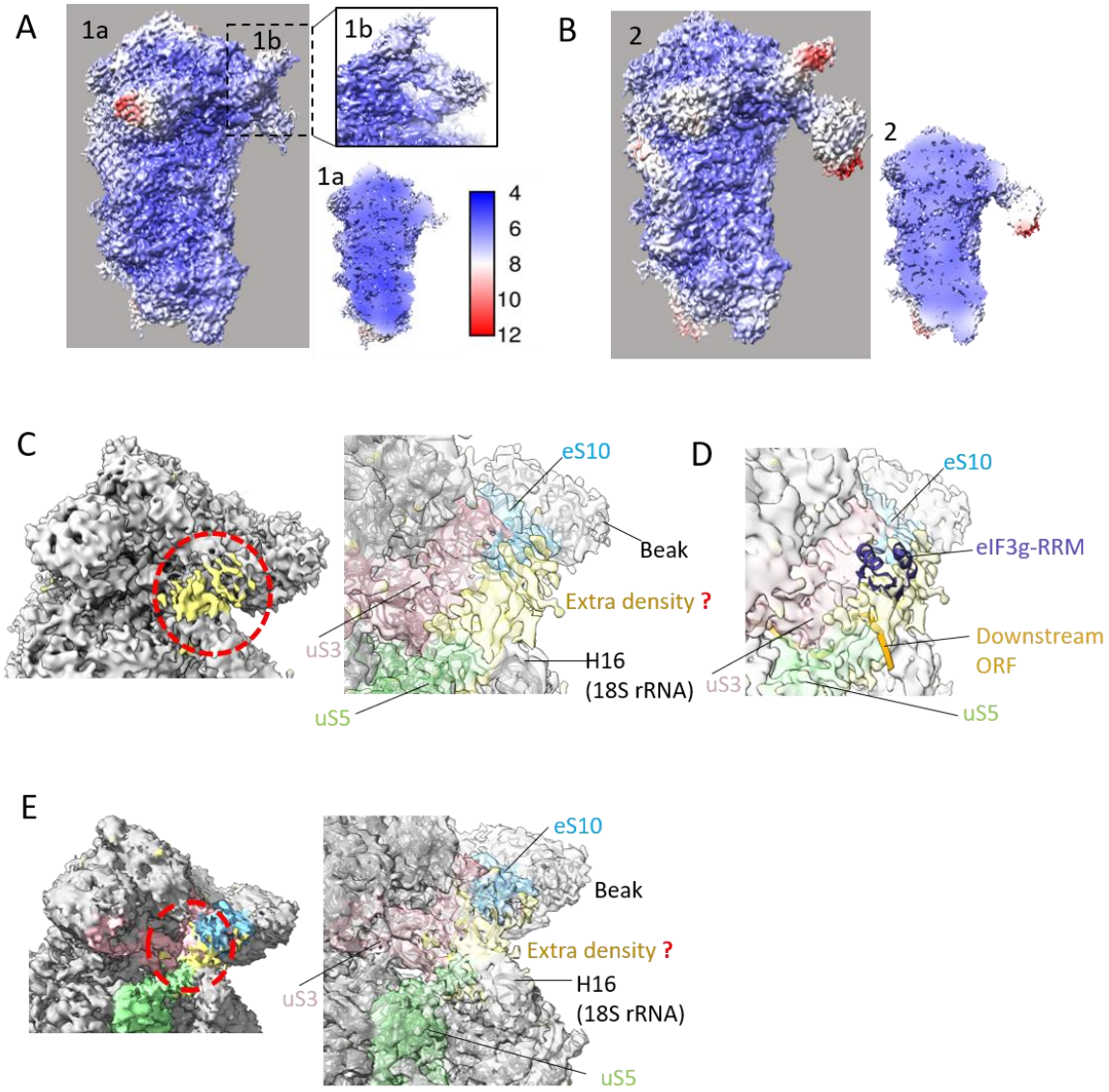

Supplementary Figure 1.2 (A) Local resolution estimation of Map B. (right) Surface view; (right-top) zoomed view on IRES density; (left-bottom) cross-section of Map B to show resolution at the core of the ribosome. **(B)** Local resolution estimation of Map B1. (right) Surface view; (left-bottom) cross-section of Map B1 to show resolution at the core of ribosome. **(C)** Extra density at the mRNA entry site of Map B/B1. Ribosomal proteins and RNA in contact with the unassigned extra density. **(D)** Superimposition of EMCV IRES-48S PIC on human 48S PIC (PDB Id- 8OZ0) shows the extra density coincides with the location of eIF3g-RRM and downstream mRNA. **(E)** Extra density at the mRNA entry site of Map A. Ribosomal proteins and RNA in contact with the unassigned extra density.

Supplementary Figure 2

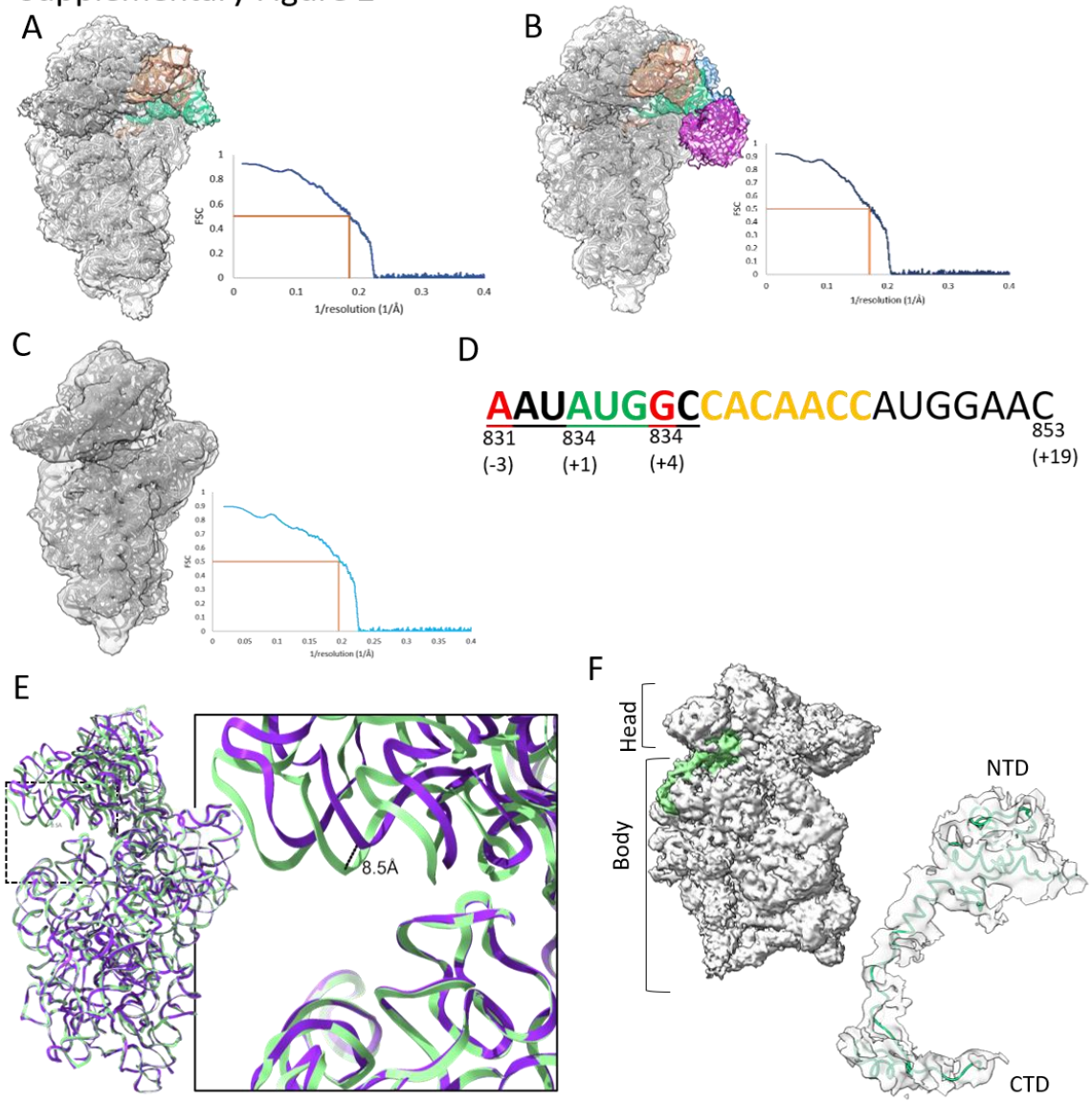

Supplementary Figure 2 (A) From Map B to model (EMCV IRES-48S PIC). Obtained Model showing 40S ribosome, RNA in channel, initiator tRNA, IRES domain. (right) Fourier Shell Correlation (FSC) of Map to Model fit. **(B)** From Map B1 to model (EMCV IRES-48S PIC). Obtained Model showing 40S ribosome, RNA in channel, initiator tRNA, IRES domain, eIF2αγ. (right) FSC of Map to Model fit. **(C)** From Map A to model by fitting of 40S ribosome without any factors. (right) FSC of Map to Model fit. **(D)** The sequence of EMCV IRES mRNA in the channel is provided. Residues in orange colour has no density in the obtained map B. **(E)** Comparing the state of 18S rRNA in Map A and Map B. **(F)** eS17-NTD position in 40S ribosome. (right) Fitting of eS17 in EMCV IRES-48S PIC map.

Supplementary figure 3

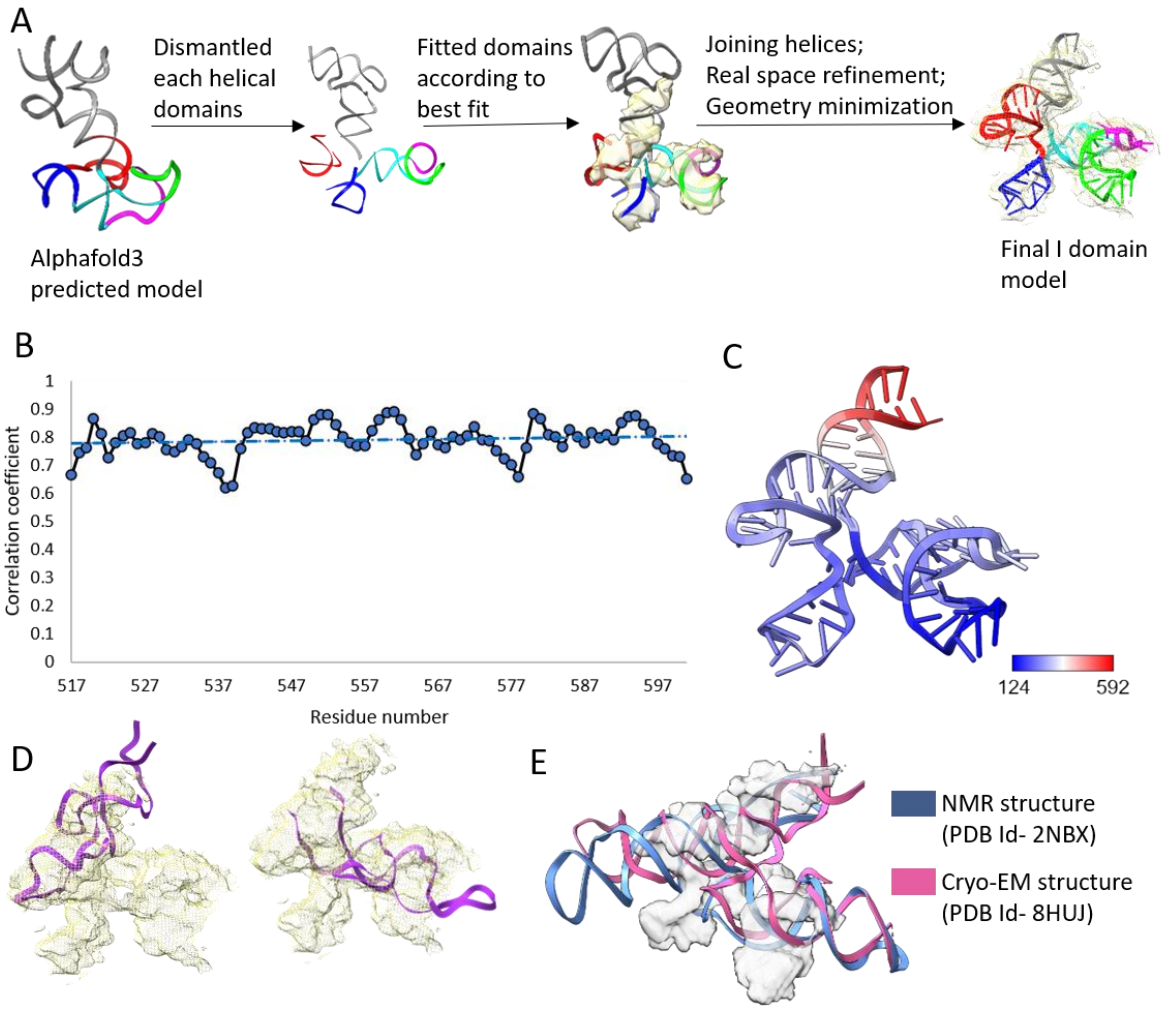

Supplementary Figure 3 (A) Process of fitting I domain apex from Alphafold3 generated model. **(B)** Correlation coefficient per residue in I domain apex for fit in the density map. **(C)** B-factor for each residue in the final model. The range is depicted in the colour key where blue is low, and red is high. **(D)** Possibility of fitting H domain in the IRES density. H domain model was generated by Alphafold3 (ptm= 0.31). **(E)** Possibility of fitting J-K domain (PDB-8HUJ) in density. The J-K domain is way too long to fit in map and does not account for certain region. The extending loops would clash with 40S ribosome and $tRNA_i$.

Supplementary Figure 4

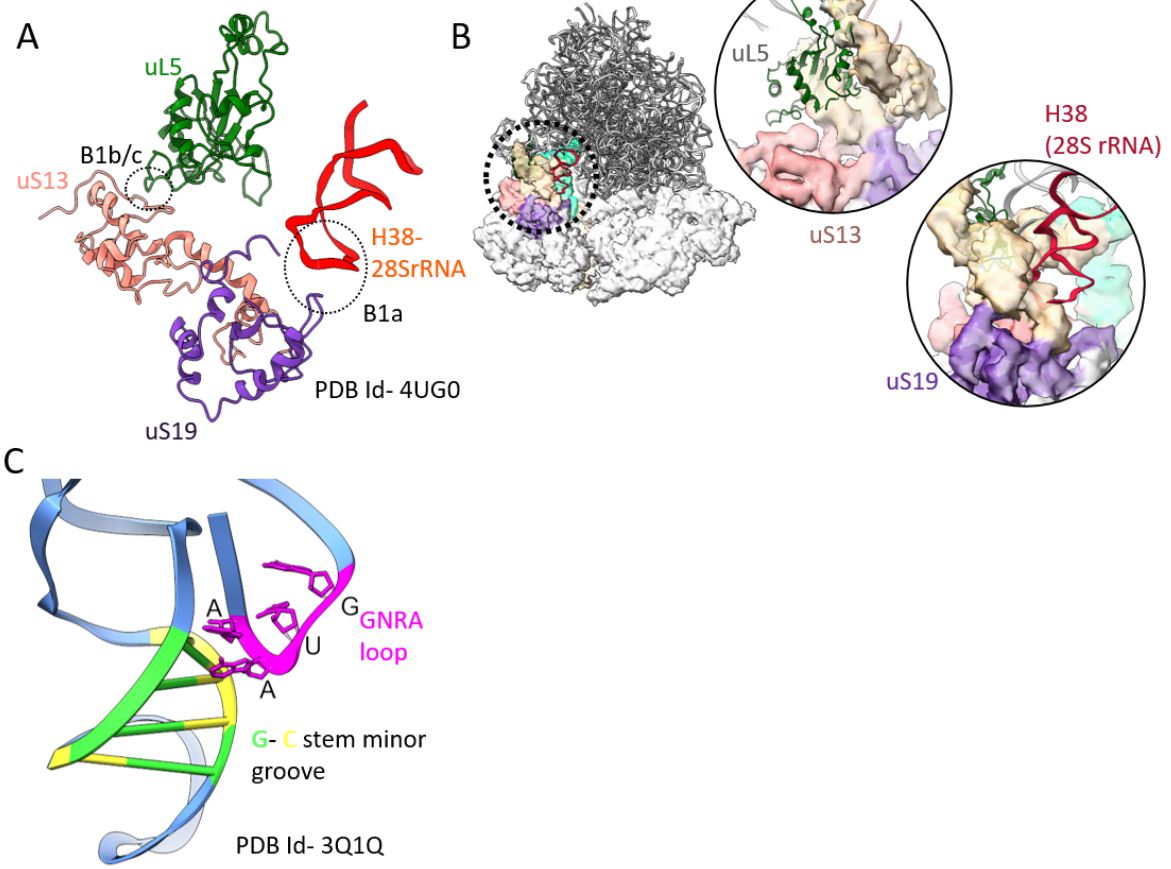

Supplementary Figure 4 (A) Interaction of uS19 and uS13 in 40S subunit with 60S subunit-Helix 38 and uL5 to form inter-subunit bridges- B1a and B1b/c, respectively in 80S (PDB Id-4UG0). **(B)** Estimation of clash with IRES domain-I during 60S joining to form 80S-elongation competent complex (PDB Id- 4UG0). uL5 and helix 38 of 28S rRNA would clash with the IRES I domain. (left) Superimposition of 80S ribosome on EMCV IRES-48S PIC. **(C)** Reported GNRA (GUGA) interaction with the minor groove formed by C-G stem in bacterial RNaseP (PDB Id-3Q1Q).

Supplementary Table 1: List of Oligos or primers used for molecular cloning

Oligo name	Sequence
PTB1_Fwd	CGGGATCCATGGACGGCATTGTCCCAGA
PTB1_Rev	CCCAAGCTTCTAGATGGTGGACTTGGAG
PTB1_3C_Fwd	CGGGATCCCTGGAGGTGCTCTTCCAGGGCCCTGGCGGCTCCATGGACGGCATTGTCCCAG
PTB1_Stop_Rev	CCCAAGCTTCTAGATGGTGGACTTGGAGAAGG
EMCV_IRES_905-Fwd	CGGGATCCCCCCCTAACGTTACTGGCC
EMCV_IRES_905-Rev	GCTCTAGAGCAGAGCATTTTGGGCATTCCTCAAAAG

Supplementary Movie 1 Legend:

The movie depicts the position of EMCV IRES (brown) on the 40S ribosomal subunit, in contact with $tRNA_i$ (green) in a 48S PIC state. On zooming, the IRES- I domain apical part is contacting the ribosomal proteins- uS13 (golden yellow) and uS19 (violet); elbow and acceptor arm of $tRNA_i$ which is base-paired to initiation codon.